molecules

MDPI

Article

Mechanofluorochromic Properties of 1,4-Diphenylanthracene Derivatives with Hypsochromic Shift

Fumihiro Kannen [1], Tadatoshi Adachi [1], Manato Nishimura [1], Kenji Yoza [2] and Takahiro Kusukawa [1,*]

[1] Faculty of Molecular Chemistry and Engineering, Graduate School of Science and Technology, Kyoto Institute of Technology, Matsugasaki, Sakyo-ku, Kyoto 606-8585, Japan
[2] Bruker Japan K.K., 3-9 Moriya-cho, Kanagawa-ku, Yokohama 221-0022, Japan
* Correspondence: kusu@kit.ac.jp

Abstract: Several types of 1,4-diphenylanthracene derivatives **1**–**4** were prepared, and their photophysical properties were observed in the solid and solution states. Interestingly, the CN-group-substituted 1,4-diphenylanthracene derivative **2** was found to exhibit a higher fluorescence quantum yield (ϕ_f = 0.71) in the solid state than in the solution state, probably due to the formation of an intermolecular Ar–CN···H–Ar hydrogen bond and antiparallel type locked packing structure in the solid state. Furthermore, for some derivatives, an increase in the fluorescence quantum yield was observed in the PMMA film (1 wt%) over both the solid state and the solution state. More interestingly, some of the 1,4-diphenylanthracene derivatives exhibited unusual mechanofluorochromic properties with a "*hypsochromic shift*" in luminous color depending on the substituents of the phenyl group, and with the derivatives having CF_3, OMe, CN, and two F substituents (**1d**–**1f**, **2**–**4**) showing a significant luminous color change with a "*hypsochromic shift*" after grinding. However, no change in the luminous color was observed for the derivatives having H, Me, and one F substituent (**1a**–**1c**), and especially for some of the CN-substituted derivatives, a reversible luminous color change with a "*hypsochromic shift*" was observed, probably due to the formation of an antiparallel type packing structure. These "*hypsochromic*" anthracene derivatives could probably be utilized as new mechanofluorochromic materials.

Keywords: mechanochromism; hypsochromic shift; anthracene; PMMA film

check for updates

Citation: Kannen, F.; Adachi, T.; Nishimura, M.; Yoza, K.; Kusukawa, T. Mechanofluorochromic Properties of 1,4-Diphenylanthracene Derivatives with Hypsochromic Shift. *Molecules* **2024**, *29*, 407. https://doi.org/10.3390/molecules29020407

Academic Editor: Barbara Panunzi

Received: 17 December 2023
Revised: 6 January 2024
Accepted: 9 January 2024
Published: 14 January 2024

Copyright: © 2024 by the authors. Licensee MDPI, Basel, Switzerland. This article is an open access article distributed under the terms and conditions of the Creative Commons Attribution (CC BY) license (https://creativecommons.org/licenses/by/4.0/).

1. Introduction

Organic solid-state light-emitting materials have received significant attention for their applications in light-emitting diodes (LEDs) [1–8], lasers [9–14], and optical waveguides [15–19]. Mechanofluorochromic materials, which are solid organic light-emitting materials that change their luminous color upon mechanical stimuli by crushing or grinding, have attracted attention for their applications in security inks, memory chips, and pressure sensors [20–30]. Numerous organic mechanofluorochromic materials have been reported, including metal complexes [31–44], anthracene derivatives [45–65], pyrene derivatives [66–76], tetraphenylethylene derivatives [77–83], and organoboron compounds [84–94]. However, most of these mechanofluorochromic materials have complex molecular structures and involve a multi-step synthesis, so the practical application of mechanofluorochromic materials with simple structures and easy synthesis is an important issue. Additionally, most of these mechanofluorochromic materials show a "*bathochromic shift*" (red shift) of their luminous color upon grinding, and mechanofluorochromic materials that show a "*hypsochromic shift*" (blue shift) in their luminous color are relatively rare [67,87,95–110].

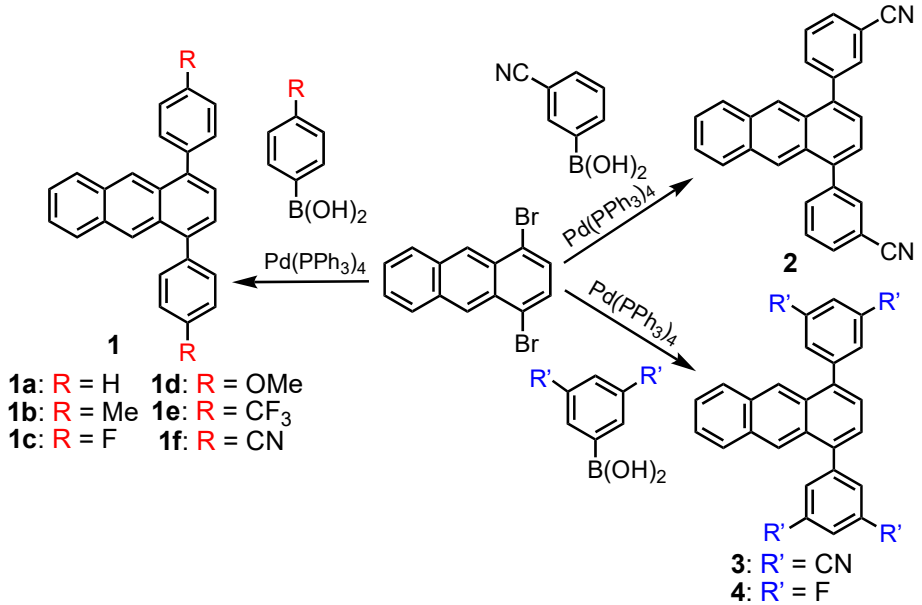
Recently, our research group reported that structurally simple 1,8-diphenylanthracene derivatives exhibit characteristic mechanofluorochromic properties with the normal "*bathochromic shift*" [62]. Interestingly, the core anthracene itself does not exhibit any

mechanofluorochromic properties at room temperature, but the introduction of phenyl substituents causes it to exhibit mechanofluorochromic properties [65]. In order to develop this structurally simple mechanofluorochromic material and to clarify the reason for the role of the substituted phenyl groups and their substitution positions (i.e., whether or not the substitution at the 1,8-positions of the phenyl group is essential), we synthesized 1,4-diphenylanthracene derivatives **1**–**4** and studied several mechanofluorochromic properties. For the mechanofluorochromic properties of the 1,4-diphenylanthracene derivatives **1a** (R = H), **1b** (R = Me), and **1c** (R = F), the blue luminous color of the pristine sample did not change after grinding. Interestingly, however, "*hypsochromic shift*" of the luminous color changes (e.g., yellow-green to blue-green) was observed after grinding for derivatives **1e**, **1f**, and **2**–**4** having OMe, CF_3, CN, and two F groups. Especially the 1,4-diphenylanthracene derivatives **1f** (R = CN), **2** (3-CN), and **3** (3,5-CN_2, R′ = CN) substituted with CN groups underwent repeated reversible luminous color changes with "*hypsochromic shift*" upon grinding, heating, and fuming with solvent vapors, although some of the derivatives could not be fully recovered. This unique "*hypsochromic shift*" with repeated reversible emission color changes is thought to be controlled by the hydrogen bonding between the Ar–CN and Ar–H groups (Ar–CN· · · H–Ar) and the formation of an antiparallel type packing structure. These unique "*hypsochromic*" anthracene derivatives could probably be applied as new mechanofluorochromic materials.

2. Results and Discussion

2.1. Synthesis and Solid-State Photophysical Properties of 1,4-Diphenylanthracene Derivatives

The 1,4-diphenylanthracene derivatives **1**–**4** were prepared from 1,4-dibromoanthracene and the corresponding phenylboronic acids using the Suzuki–Miyaura cross-coupling reaction catalyzed by $Pd(PPh_3)_4$ (Scheme 1), and all the derivatives were obtained in 45–99% yields (see experimental part).



Scheme 1. Synthetic route of 1,4-diphenylanthracene derivatives **1**–**4** (Red is substituent R and blue is substituent R′).

The photophysical properties of the obtained 1,4-diphenylanthracene derivatives (**1**–**4**) in the solid and solution state are shown in Table 1, Figures S1, S2, and S15, and the absorption spectra are shown in Figures S13 and S14. All the synthesized 1,4-diphenylanthracene derivatives **1**–**4** showed a light-blue (LB), green (G), or yellow-green (YG) luminous color in the pristine solid state (λ_{max} = 452–536 nm) under UV irradiation at 365 nm (Table 1, Figure S2). For the solid-state fluorescence spectra of the pristine samples of the 1,4-diphenylanthracene derivatives, the fluorescence bands around 455–480 nm (λ_{max}) were

observed in the light-blue luminous solids (**1a**–**1c**, LB, Table 1, Figures 1a, S1 and S2). On the other hand, in the yellow-green luminous solids (**1d**, **1f**, **2**, **3**, YG), the fluorescence bands were observed around 514–522 nm (λ_{max}). Additionally, for the green luminous solids (**1e**, **4**, G), two fluorescence bands were observed around 480 and 530 nm (λ_{max}, Table 1, Figures 1b, S1 and S2).

Table 1. Fluorescence properties of 1,4-diphenylanthracene derivatives.

Compounds	λ_{max}/nm [a], Luminous Color [b]			Φ_f [c]		τ [d]/ns	
	Pristine	Ground	Solution [e]	Pristine (Ground)	Solution [f]	Pristine (Ground)	Solution [f]
1a (R = H)	455, 480, LB	448, 481, LB	422, 438, B	0.20 (0.23)	0.47	2.27 (6.48)	3.02
1b (R = Me)	455, 480, LB	450, 483, LB	432, 443, B	0.31 (0.21)	0.49	3.96 (13.4)	3.08
1c (R = F)	452, 480, LB	448, 482, LB	421, 437, B	0.24 (0.25)	0.49	3.05 (13.7)	3.36
1d (R = OMe)	515, YG	486, BG	454, LB	0.15 (0.18)	0.40	12.4 (10.4)	2.69
1e (R = CF_3)	497, 530, G	488, BG	438, 440, B	0.37 (0.33)	0.51	4.69 (7.63)	2.76
1f (R = CN)	514, YG	497, G	458, LB	0.26 (0.33)	0.55	32.8 (18.4)	2.57
2 (3-CN)	522, YG	493, BG	428, 439, B	0.71 (0.37)	0.46	109 (91.5)	2.85
3 (R′ = CN)	518, YG	497, G	455, LB	0.15 (0.05)	0.41	7.39 (4.09)	2.57
4 (R′ = F)	489, 536,G	489, BG	426, 438, B	0.44 (0.22)	0.50	5.22 (5.36)	2.90

[a] Solution and solid-state emission (λ_{ex} = 365 nm). [b] Luminous color, B: blue, G: green, BG: blue-green, LB: light-blue, YG: yellow-green under 365 nm UV irradiation. [c] Fluorescence quantum yield determined by a calibrated integrating sphere at λ_{ex} = 365 nm. [d] Averaged fluorescence lifetime at λ_{ex} = 365 nm. [e] $CHCl_3$ solution (25 μM, λ_{ex} = 365 nm). [f] $CHCl_3$ solution (10 μM) after Ar bubbling.

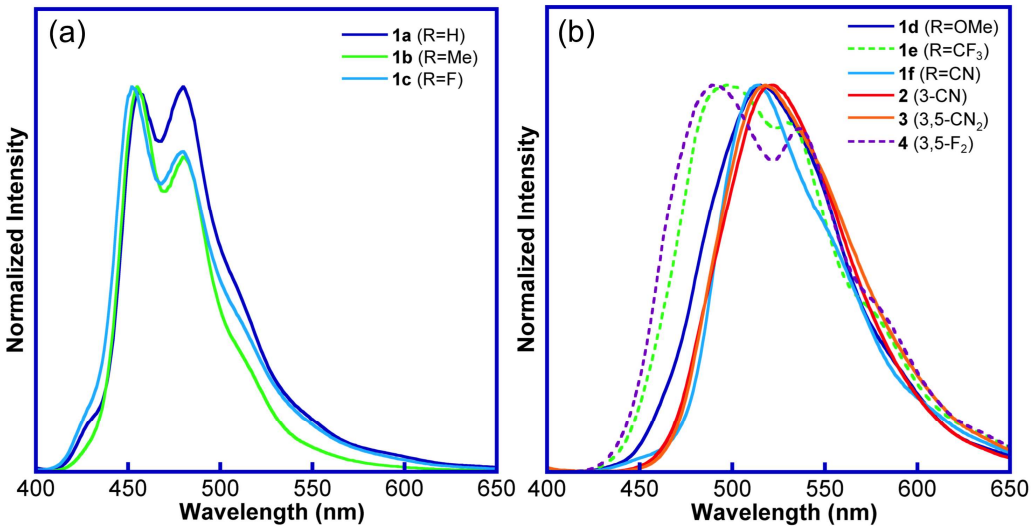


Figure 1. Fluorescence spectra of 1,4-diphenylanthracene derivatives (pristine solids, λ_{ex} = 365 nm). (**a**) 1,4-diphenylanthracene derivatives **1a**–**1c** (LB), (**b**) 1,4-diphenylanthracene derivatives **1d**–**1f**, **2**–**4** (YG: solid line, G: dotted line).

The fluorescence quantum yields (Φ_f) of the 1,4-diphenylanthracene derivatives were 0.15–0.71 in the pristine solids, and a relatively high fluorescence quantum yield was observed for **2** (3-CN, Φ_f = 0.71). The fluorescence lifetimes of the light-blue luminous crystals of **1a**–**1c** are 2.27–3.96 ns, indicating that the short lifetimes are probably due to the monomer emission of the diphenylanthracene part (Table 1, Figure S20). On the other hand, slightly longer fluorescence lifetimes (4.69–5.22 ns) were observed for the green luminous crystals (**1e**, **4**). Additionally, much longer fluorescence lifetimes (7.39–109 ns) were observed for the yellow-green luminous crystals (**1f**, **2**, **3**), and these greenish emission bands are probably due to the excimer emission of the diphenylanthracene part [47,48,51,61–65].

To understand the relationship between the crystal packing and solid state photophysical properties (fluorescence quantum yield, fluorescence lifetime, and luminous color) of

the 1,4-diphenylanthrcene derivatives, the single crystal structures of **1a** (R = H, light-blue luminous color, LB), **1b** (R = Me, light-blue luminous color, LB), **1c** (R = F, light-blue luminous color, LB), **1d** (R = OMe, yellow-green luminous color, YG), **1f** (R = CN, yellow-green luminous color, YG), and **2** (3-CN, yellow-green luminous color, YG) were analyzed. Single crystals were obtained from dimethoxyethane (DME) solutions for **1d** and **1f**, from hexane solutions for **1a** and **1c**, from a $CHCl_3$ solution for **2**, and from a CH_2Cl_2 solution for **1b**. For the bimolecular stacked crystal packing of **1a** (R = H), **1b** (R=Me), **1c** (R = F), and **1d** (R = OMe), the 1,4-diphenylanthracene rings are arranged in the same direction, called the "parallel orientation" (Figure 2). On the other hand, in the bimolecular stacked crystal packing of the CN-group substituted derivatives **1f** (R = CN) and **2** (3-CN), the 1,4-diphenylanthracene rings are arranged in the "antiparallel orientation", and a stronger π-stacking is observed than in the "parallel orientation" (Figure 2). Additionally, Ar–CN$\cdots$H–Ar or Ar–F$\cdots$H–Ar hydrogen bonds were observed in the crystal packing of **1c** (R = F), **1f** (R = CN), and **2** (3-CN) with CN or F substituents (Figures S28, S32 and S34). To understand the reason for the formation of the "parallel" and "antiparallel" orientation packings of the 1,4-diphenylanthracene rings in the crystal structure, the electrostatic potential surfaces were calculated using DFT calculations according to the obtained crystal data (Figures S41 and S42). For the CN-group substituted derivatives **1f** (R = CN) and **2** (3-CN), the positive charges are located at the edge of the substituted phenyl ring, as shown in Figures S41 and S42, and these positively charged edges are stacked with the center part of the phenyl ring of the other molecules to form a stable stacking bimolecular "antiparallel" packing. Additionally, in the crystal structure of the bimolecular packing of **1f** (R = CN) and **2** (3-CN), many interactions, such as CH–π interactions between two 1,4-diphenylanthracen rings, were observed compared to the other non-CN substituted derivatives (**1a**–**1d**), as shown in Figure S36, and it may be showing that the "antiparallel" orientation is more stable than the "parallel" orientation in the case of electron withdrawing CN-group substituted derivatives.

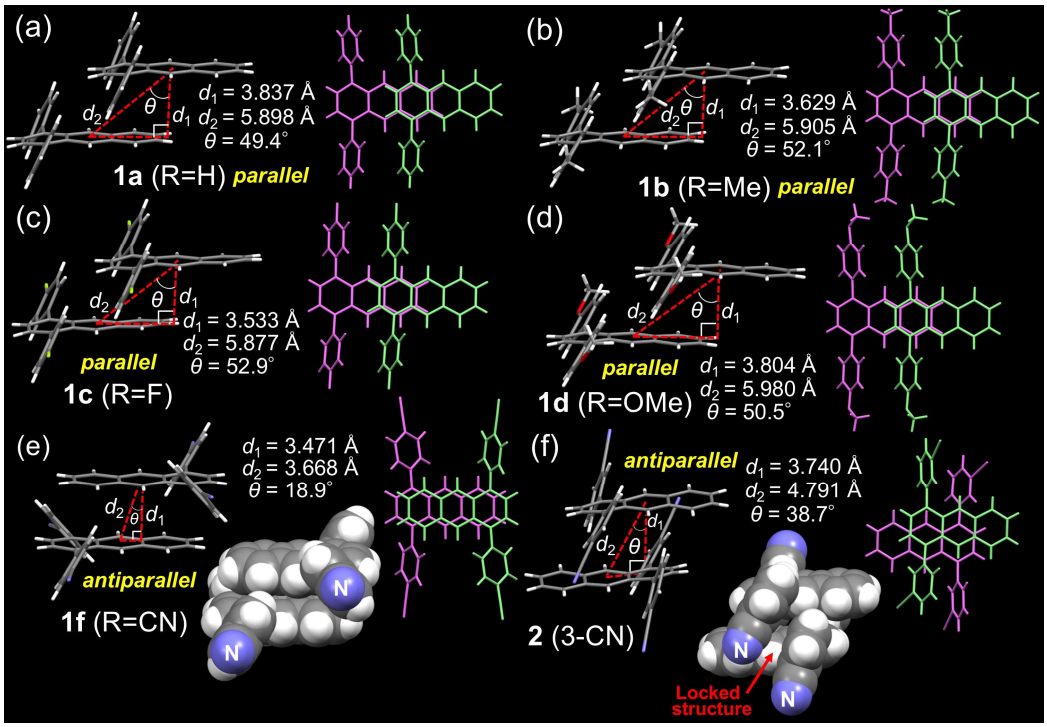


Figure 2. Crystal structures of the 1,4-diphenylanthracene derivatives: (**a**) **1a** (R = H), (**b**) **1b** (R = Me), (**c**) **1c** (R = F), (**d**) **1d** (R = OMe), (**e**) **1f** (R = CN), (**f**) **2** (3-CN).

According to the crystal structure analysis and photophysical data of the 1,4-diphenylanthracene derivatives, we can discuss the following:

(1) *Relation between solid-state luminous color, crystal packing, Hirshfeld surface analysis, and fluorescence lifetimes*: As already mentioned, the luminous colors of the pristine samples of the 1,4-diphenylanthracene derivatives show light-blue (**1a**–**1c**, LB), green (**1e**, **4**, G), and yellow-green (**1d**, **1f**, **2**, **3**, YG) colors. In the case of the light-blue luminous derivatives **1a**–**1c**, the emission is probably derived from the monomer of the 1,4-diphenylanthracene rings since the crystal packing of **1a**–**1c** showed only partial overlapping of the anthracene ring, as indicated by the purple and green colors in Figure 2a,c. On the other hand, in the case of the yellow-green luminous derivatives **1f** (R = CN) and **2** (3-CN), the emission is probably derived from the excimer state of the 1,4-diphenylanthracene rings, and a greater overlapping of the anthracene rings compared to **1a**–**1c** is observed, as shown in Figure 2e,f. In the case of the yellow-green luminous MeO-group substituted derivative **1d**, the crystal packing is very similar (overlapping only one benzene ring) to the light-blue luminous derivatives **1a**–**1c,** as shown in Figure 2a–d, suggesting that an intermolecular charge transfer may be operating (see Figures S39 and S40, DFT calculation) and showing a yellow-green luminous color. To further understand the contribution of the π–π stacking for the crystal packing, the Hirshfeld surface analysis according to the crystal data was performed (Figure 3). The contribution of π–π stacking for **1f** (R = CN, contribution of the C–C interactions: 13.8%) and **2** (3-CN, contribution of the C–C interactions: 13.5%) is greater than that for **1a**–**1c** (contribution of the C–C interactions: 6.4–9.8%), indicating that the yellow-green emission of **1f** and **2** is due to the formation of the π–π stacking (excimer emission). The fluorescence lifetimes of the 1,4-diphenylanthracene derivatives for the pristine state also show the difference in the contribution of the π–π stacking interactions as follows. Short fluorescence lifetimes between 2.27–3.96 ns were observed for the light-blue luminous samples **1a**–**1c**; however, slightly longer fluorescence lifetimes were observed for the green luminous samples **1e** (4. 69 ns, R = CF_3) and **4** (5.22 ns, R′ = F, 3,5-F_2) and for the yellow-green luminous samples **1f** (R = CN), **2** (3-CN) and **3** (R ′= CN, 3,5-CN_2), longer fluorescence lifetimes were observed between 7.39 and 109 ns (Table 1, Figure S20). These observed fluorescence lifetimes are increasing in the order of light-blue < green < yellow-green luminous color (the fluorescence wavelengths also increased in the same order). These results indicated that the contribution of the π–π stacking interactions is also increasing in the same order, which is in good agreement with the crystal data only except for **1d**.

(2) *Relation between fluorescence quantum yield, fluorescence lifetime, and crystal packing of **1f** (R=CN) and **2** (3-CN)*: The pristine sample of **2** (3-CN) exhibited a relatively high fluorescence quantum yield (ϕ_f = 0.71) compared to the other 1,4-diphenylanthracene derivatives (ϕ_f = 0.15–0.44, Table 1), as already described. To consider the reason for the higher fluorescence quantum yield of **2** (3-CN), we calculated the rate constant k_f for the fluorescence and the rate constant k_{nr} for non-radiative decay (Table S1) and compared k_f and k_{nr} to that of **1f** (R = CN) and **2** (3-CN). The rate constants k_f for the fluorescence of **1f** (k_f = 0.008 ns^{-1}) and **2** (k_f = 0.006 ns^{-1}) were almost the same, but the rate constant k_{nr} for the non-radiative decay of **2** (k_{nr} = 0.003 ns^{-1}) was about seven times lower than that of **1f** (k_{nr} = 0.022 ns^{-1}), and the difference in k_{nr} caused the fluorescence quantum yield of **2** (ϕ_f = 0.71) to be higher than that of **1f** (ϕ_f = 0.26) in the pristine solid state. The difference in k_{nr} between **1f** and **2** may be due to the difference in the crystal packing structure. Due to the substitution of a CN group at the 3-position (meta-position) of the phenyl group in the derivative **2** and the intermolecular hydrogen bond (Ar–CN$\cdots$H–Ar) formed by the CN group, the crystal packing structure of **2** forms a tight, lock-and-key type packing compared to the loose packing structure of **1f** (Figures 2e,f and S37). The tight packing structure of **2** is considered to suppress the molecular vibration in the solid state compared to

the packing structure of **1f** and exhibits a very low k_{nr} (0.003 ns^{-1} for **2**) and a high fluorescence quantum yield (ϕ_f = 0.71).

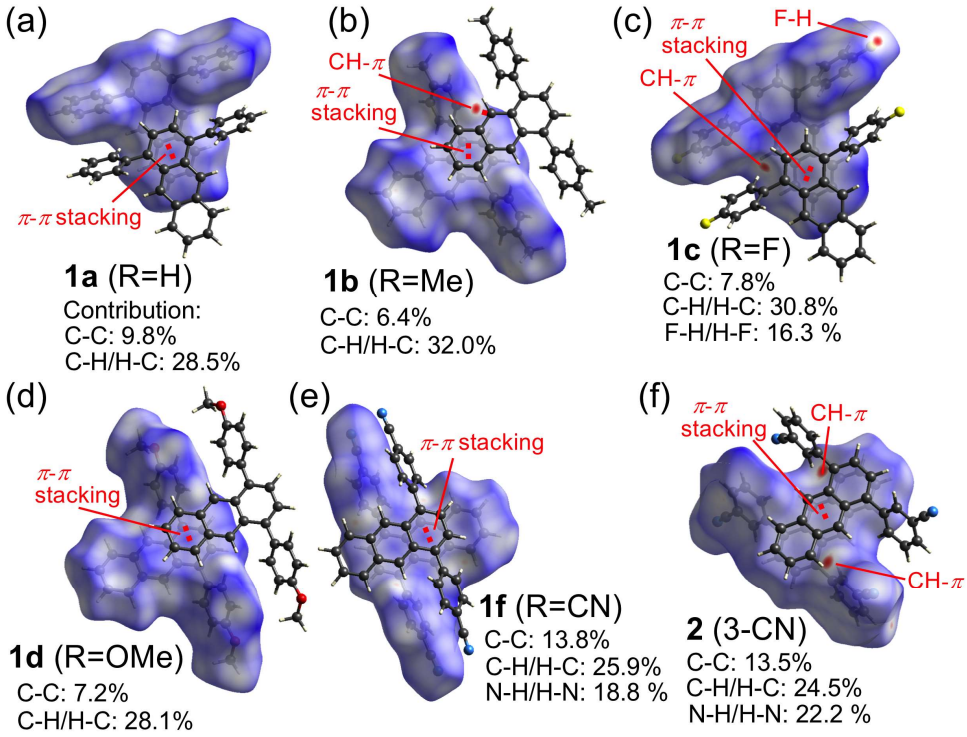


Figure 3. Hirshfeld surface showing the intermolecular interactions over d_{norm} and the percentages of the contact's contribution to the total Hirshfeld surface area of the molecules: (**a**) **1a** (R = H), (**b**) **1b** (R = Me), (**c**) **1c** (R = F), (**d**) **1d** (R = OMe), (**e**) **1f** (R = CN), (**f**) **2** (R′ = CN, 3-CN).

2.2. Photophysical Properties of 1,4-Diphenylanthracene Derivatives in Solution and in PMMA Films

To compare the photophysical properties of the 1,4-diphenylanthracene derivatives in the solid and solution states, we measured their UV spectra, fluorescence spectra, fluorescence quantum yields, and fluorescence lifetimes of the 1,4-diphenylanthracene derivatives in chloroform solutions (Table 1, Figures S14–S16 and S21). In the case of 1,4-diphenylanthracene derivatives **1a**–**1c**, **1e**, **2,** and **4**, a blue luminous color (421–443 nm) was observed in the $CHCl_3$ solution. However, for derivatives **1d** (R = OMe), **1f** (R = CN), and **3** (3,5-CN_2), which have electron-donating and electron-withdrawing groups, a light-blue luminous color (454–458 nm) was observed in the $CHCl_3$ solution (Figures S15 and S16). These derivatives may be causing a charge-transfer interaction in the solution state, but only a small solvatochromic effect on the fluorescence spectra was observed in different solvents (Figure S17). For all the 1,4-diphenylanthracene derivatives, the fluorescence quantum yields were observed with a moderate efficiency around ϕ_f = 0.41–0.56, and for almost all derivatives, the $CHCl_3$ solution state showed higher fluorescence quantum yields than the pristine solid state. Additionally, the fluorescence lifetimes were observed around τ = 2.57–3.36 ns for all the derivatives, probably indicating a monomer emission in the solution state. Interestingly, only derivative **2** (3-CN) showed a higher fluorescence quantum yield (ϕ_f = 0.71) in the pristine solid state than in the solution state (ϕ_f = 0.46 in $CHCl_3$).

In order to develop new fluorescent materials, it is important that the newly synthesized fluorescent materials exhibit high fluorescence properties even in the polymer-supported solid state. Therefore, we measured the photophysical properties of the 1,4-diphenylanthracene derivatives in PMMA (polymethyl methacrylate). The desired 1,4-diphenylanthracene derivative-containing PMMA film (1 wt%) was prepared by casting on a glass plate using a $CHCl_3$ solution. For most of the PMMA films obtained, a blue

or light-blue luminous color was observed, and the fluorescence spectra was similar to that of the $CHCl_3$ solution but was significantly different from that of the pristine solid (Figures S18 and S19). These observations indicated that the blue emission of the 1,4-diphenylanthracene derivatives in the PMMA films is derived from the monomer emission, which is a significant difference from the solid-state emission (Figure S18). The fluorescence quantum yields of the PMMA films (1 wt%) of the 1,4-diphenylanthracene derivatives show relatively high efficiencies around ϕ_f = 0.62–0.71. Interestingly, the fluorescence quantum yields in the PMMA films are increased compared to the solid and solution states, except for **2** (3-CN). Additionally, the fluorescent lifetime of the PMMA film (1 wt%) of the 1,4-diphenylanthracene derivatives exhibited a slightly longer lifetime (τ = 3.45–4.16 ns) than the solution state (Tables S1 and S2, Figure S22). Based on these photophysical measurements, the rate constant k_f for fluorescence of the PMMA films (k_f = 0.1425–0.2058) was found to be similar to that of the corresponding solution state (Tables S1 and S2). However, the rate constants k_{nr} for non-radiative decay of the PMMA film (k_{nr} = 0.0837–0.0936) was found to be much lower than for the solution and solid states (Tables S1 and S2). The lower k_{nr} value showed the inhibition of the molecular motion in the PMMA film and showed an increasing fluorescence quantum yield in the PMMA films than in the solution state. In the pristine solid state of the 1,4-diphenylanthracene derivatives, the aggregation-caused quenching (ACQ) effect that may have occurred and the fluorescence quantum yields were reduced, except for derivative **2** (3-CN).

2.3. Mechanofluorochromic Properties of 1,4-Diphenylanthracene Derivatives

To further investigate the fluorescence properties of these 1,4-diphenylanthracene derivatives, we studied their mechanofluorochromic properties in the solid state. The light-blue luminous color (λ_{max} = 452–455, 480 nm) of the pristine samples of the 1,4-diphenylanthracene derivatives **1a** (R = H), **1b** (R = Me), and **1c** (R = F) did not change their luminous color after grinding in a mortar at room temperature under 365 nm UV light (Table 1, Figures 4, S1 and S2). On the other hand, the yellow-green or green luminous color of the 1,4-diphenylanthracene derivatives **1d** (R = OMe, from 515 nm YG to 486 nm BG), **1e** (R = CF_3, from 497, 530 nm G to 488 nm BG), **1f** (R = CN, from 514 nm YG to 497 nm G), **2** (3-CN, from 522 nm YG to 493 nm BG), **3** (3,5-CN_2, R′ = CN, from 518 nm YG to 497 nm G), and **4** (3,5-F_2, R′ = F, from 489, 536 nm G to 489 nm BG) changed to shorter wavelength luminous colors (i.e., *hypsochromic shift*) when ground in a mortar (Table 1, Figures 4, 5a, S1 and S2), and the fluorescence spectra also significantly changed, as shown in Figure S1. The compounds that show a "hypsochromic shift" in fluorescent color after grinding are very rare and interesting, but compared to mechanofluorochromic materials that show a "bathochromic shift", the mechanistic studies are unclear at the present moment [67,87,95–110].

For the mechanofluorochromic properties of the 1,8-diphenylanthracene derivatives previously reported, some of the derivatives recovered to their original fluorescent color after grinding within 5 min. at room temperature, but the CN-group substituted derivatives did not recover to their original emission color at room temperature [62]. However, this mechanofluorochromism of the 1,4-diphenylanthracene derivatives was not observed as a self-recovering phenomenon within 5 min. at room temperature in the luminous color changed derivatives **1d**–**1f** and **2**–**4** (Figures S1 and S2).

For the yellow-green (YG) emitting CN-substituted derivatives **1f**, **2,** and **3**, the fluorescence lifetimes (τ) of the ground samples became shorter than those of the pristine samples (Table 1), along with a "*hypsochromic shift*" of the luminous color. These results indicated that the π–π stacking structure dissociates after grinding, exhibiting a "*hypsochromic shift*" in the luminous color and a shortening of the fluorescence lifetimes.

To further understand the mechanofluorochromism of the 1,4-diphenylanthracene derivatives, the UV and IR spectra were observed in the solid state for the pristine and ground samples. In the UV spectra, a blue shift (*hypsochromic shift*) and decreasing of the longer wavelength peaks were observed for the derivatives **1d**–**1f**, **2**–**4** (Figures 5b and S13),

which showed a "*hypsochromic shift*" in the fluorescence spectra after grinding, indicating a decrease in the contribution of the π-stacking structure after grinding. Furthermore, infrared (IR) spectra of the CN-substituted 1,4-diphenylanthracene derivatives **1f** (R = CN) and **2** (3-CN) before and after grinding were observed, and the CN stretching band of the **1f** and **2** shifted to the higher wavenumber side from the pristine to ground one, indicating that the hydrogen bond (Ar–CN$\cdots$H–Ar) strength decreased after grinding (Figures 6, S10 and S11).

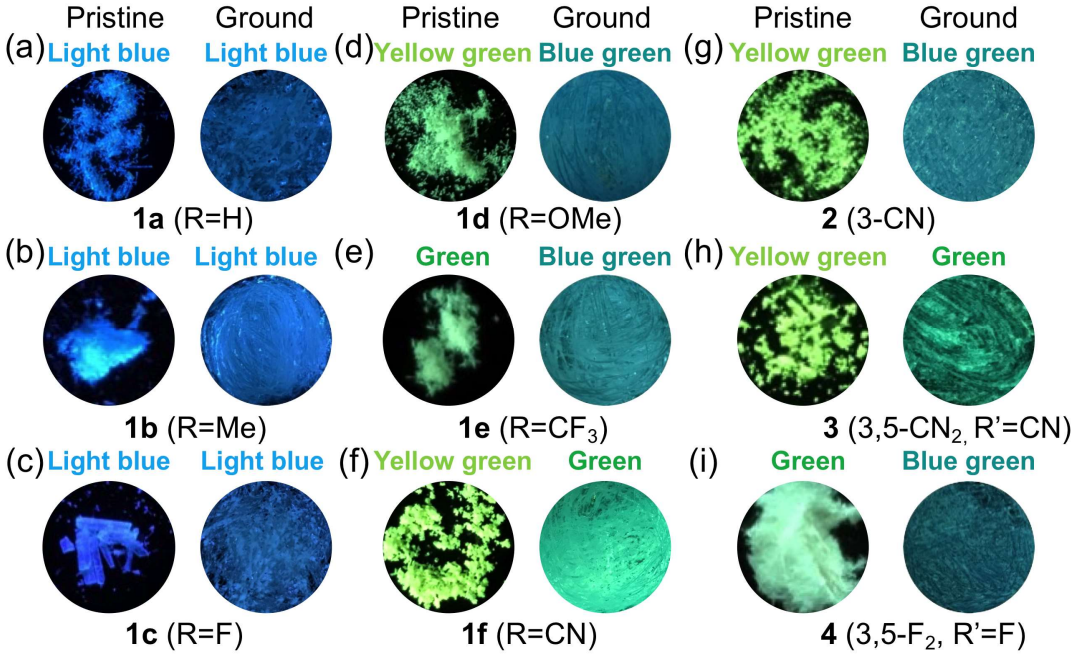


Figure 4. Fluorescent images of the pristine and ground samples of 1,4-diphenylanthracene derivatives **1**–**4** during a 365 nm UV irradiation: (**a**) **1a** (R = H), (**b**) **1b** (R = Me), (**c**) **1c** (R = F), (**d**) **1d** (R = OMe), (**e**) **1e** (R = CF_3), (**f**) **1f** (R = CN), (**g**) **2** (3-CN), (**h**) **3** (3,5-CN_2, R′ = CN), (**i**) **4** (3,5-F_2, R′ = F).

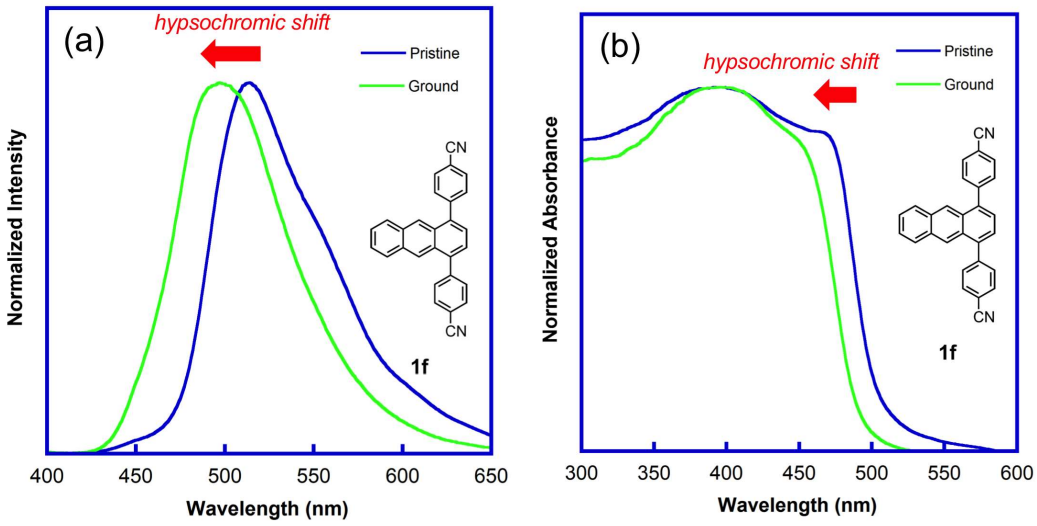


Figure 5. Fluorescence and UV-vis spectra of 1,4-diphenylanthracene derivative **1f** (R=CN) in the solid state: (**a**) fluorescence spectra of the pristine and ground samples (λ_{ex} = 365 nm), (**b**) UV-vis absorption spectra of the pristine and ground samples.

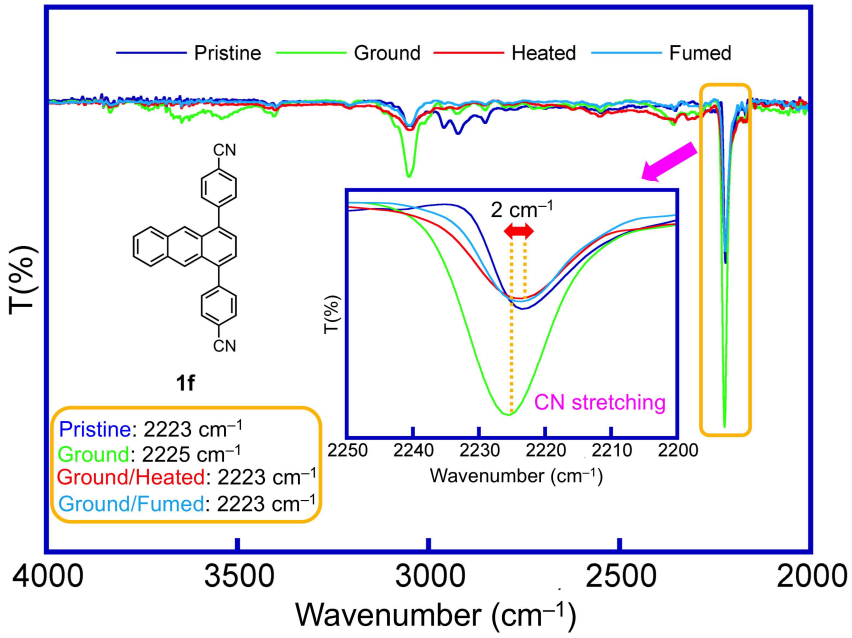


Figure 6. IR spectra of the 1,4-diphenylanthracene derivative **1f** (pristine, ground, ground-heated, ground-fumed samples) in the CN stretching region.

2.4. Vapochromic and Thermochromic Properties of 1,4-Diphenylanthracene Derivatives

To understand the reversibility of the luminous color of the 1,4-diphenylanthracene derivatives, fluorescence images and fluorescence spectra of the ground samples were observed after fuming with the CH_2Cl_2 vapor. The blue-green luminescent ground samples of derivatives **1d** (R = OMe), **1e** (R = CF_3), and **4** (3,5-F_2, R′ = F) showed no recovery of the luminous color (recovery to green or yellow-green, bathochromic shift) after fuming with the CH_2Cl_2 vapor for 20 h (Figures S3 and S4). Interestingly, for the CN-group-substituted 1,4-diphenylanthracene derivatives **1f** (R = CN), **2** (3-CN), and **3** (3,5-CN_2, R′ = CN), the yellow-green luminous color of the pristine sample turned to the green or blue-green luminous color ("*hypsochromic shift*") with grinding, and the original yellow-green luminous color was recovered by fuming with solvent vapor (Figures 7, S3 and S4). Additionally, repeated grinding–fuming cycles were also observed, but in some cases, a decrease in the fluorescence intensity and decreasing of the color-switching ability were observed (Figures 8, S5 and S6). To understand the reason for the decrease in the fluorescence intensity and decreasing of the color-switching ability, we measured fluorescence spectra and ^{1}H NMR spectra of the derivatives **1a** (R = H) and **2** (3-CN) after UV irradiation in the solid state (365 nm, 5 min.). In the fluorescence spectra of **1a**, no change in fluorescence intensity was observed after 365 nm UV irradiation. On the other hand, a slight decrease in fluorescence intensity was observed for derivative **2**, but no spectral change was observed in the ^{1}H NMR spectrum after dissolving the irradiated samples (Figures S43 and S44).

Again, for derivatives **1d** (R = OMe), **1e** (R = CF_3), and **4** (3,5-F_2, R′ = F), no recovery to the original luminous color (pristine state) by heating the ground sample was observed (Figures S3 and S4). However, for the CN-group-substituted 1,4-diphenylanthracene derivatives **1f** (R = CN), **2** (3-CN), and **3** (3,5-CN_2, R′ = CN), a similar recovery of the luminous color of the ground sample to the luminous color of the pristine sample by heating was also observed (Figures 7, S3, S4, and S7–S9). The green luminous ground sample of **1f** (R = CN) turned yellow-green when heated at 80 °C for 5 min., a recovery of the green luminous color was observed upon regrinding (Figures 7 and 8a), and the repeated cycles of grinding–heating are shown in Figure 8c. Although repeated grinding–heating cycles were observed, in some cases, a decrease in the fluorescence intensity and decreasing of the color-switching ability were observed.

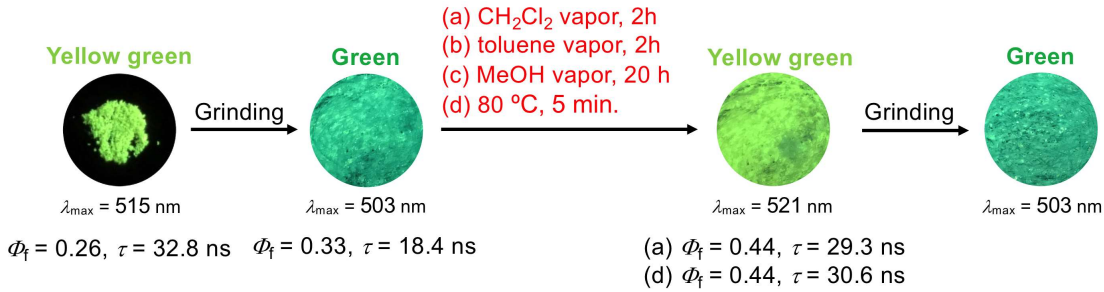


Figure 7. Typical fluorescence images of ground, fumed (CH_2Cl_2, toluene, and MeOH vapors), and heated (80 °C for 5 min.) samples of 1,4-diphenylanthracene derivative **1f** (R = CN) upon irradiation by 365 nm UV lamp.

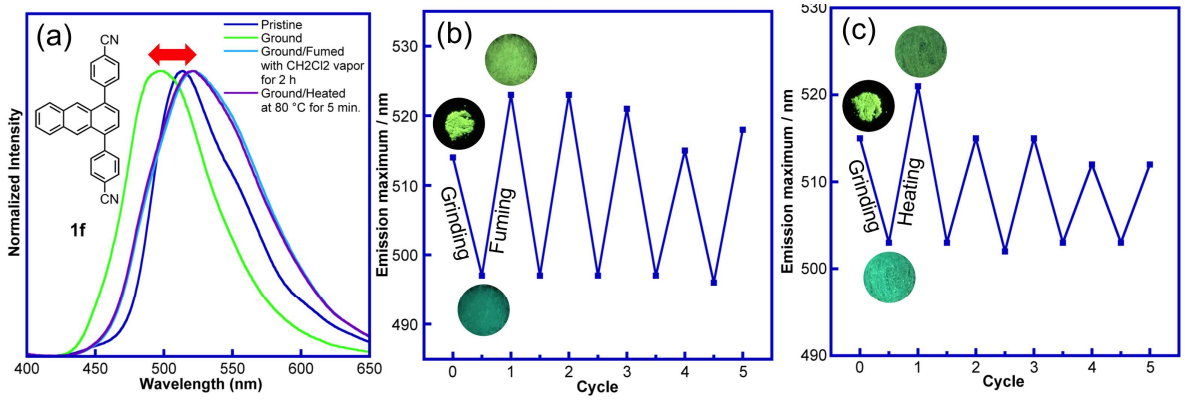


Figure 8. Vapochromic and thermochromic properties of 1,4-diphenylanthracene derivative **1f** (R = CN): (**a**) fluorescence spectra of pristine, ground, ground-fumed (CH_2Cl_2 vapor, 2 h), and ground-heated (80 °C, 5 min.) samples, (**b**) repeated grinding–fuming cycles, (**c**) repeated grinding–heating cycles.

To further understand the grinding–heating process of the CN-substituted 1,4-diphenylanthracene derivative **1f** (R = CN), differential scanning calorimetry (DSC) was conducted to observe the phase transition between the ground and ground-heated samples. For the yellow-green luminous pristine sample of **1f**, only the endothermic peak of melting (281.6 °C, 285.9 °C) was observed (Figure 9a). On the other hand, a broad exothermic peak was observed around 89.1 °C in the green luminous ground sample, which may have caused the transition from the green to yellow-green luminous state. Similar exothermic peaks were also observed in the ground samples for derivative **2** with a substituted CN group (Figure 9b). The DSC analysis of the other 1,4-diphenylanthracene derivatives **1a**–**1e** was examined, but only endothermic melting peaks were observed (Figure S12).

To understand in detail the mechanofluorochromic properties of the 1,4-diphenylanthracene derivatives, the powder X-ray diffraction patterns (PXRD) of the pristine, ground, ground-fumed, and ground-heated samples of derivative **1f** (R = CN) were observed. The "yellow-green" luminous pristine sample of **1f** showed a sharp and strong peak in the PXRD measurement (Figure 10a), but no diffraction peak was observed in the ground "green luminous" sample (Figure 10b). After heating at 80 °C for 5 min., the ground sample recovered its "yellow-green luminous color" and showed small crystallization peaks (Figure 10c). Similar crystallization of the ground sample was also observed when fuming with CH_2Cl_2 vapor for 2 h (Figure 10d). These observations, like those in the previously reported paper, show that this mechanofluorochromism may be operating under a phase transition from the crystalline state to the amorphous state [32–44,46–49,52,53,55,57–59,71,72,77,80,83,84,86,87,89–94]. Furthermore, during the vapochromic and thermochromic recovery of the ground sample of **1f**, a reversible change in the fluorescence lifetimes (pristine: τ = 32.8 ns, ground: τ = 18.4 ns, ground-fumed with CH_2Cl_2 vapor: τ = 29.3 ns, ground-heated: τ = 30.6 ns)

was observed (Figure 7). These changes in the fluorescence lifetimes of **1f** are indicated as follows: (i) the π–π stacked pristine sample showed a yellow-green luminous color (λ_{max} = 514 nm) and showed a longer fluorescence lifetime (τ = 32.8 ns) due to π–π stacking structure; (ii) after grinding, the sample showed a green luminous color (λ_{max} = 497 nm, "*hypsochromic shift*") and showed a shorter fluorescence lifetime (τ = 18.4 ns) due to the decreasing of the π–π stacked structure; (iii) after fuming and heating of the ground sample, the longer fluorescence lifetimes (τ = 29.3 and 30.6 ns) and yellow-green luminous color were recovered due to the recovering of the π–π stacked structure (crystallization was observed in the PXRD analysis).

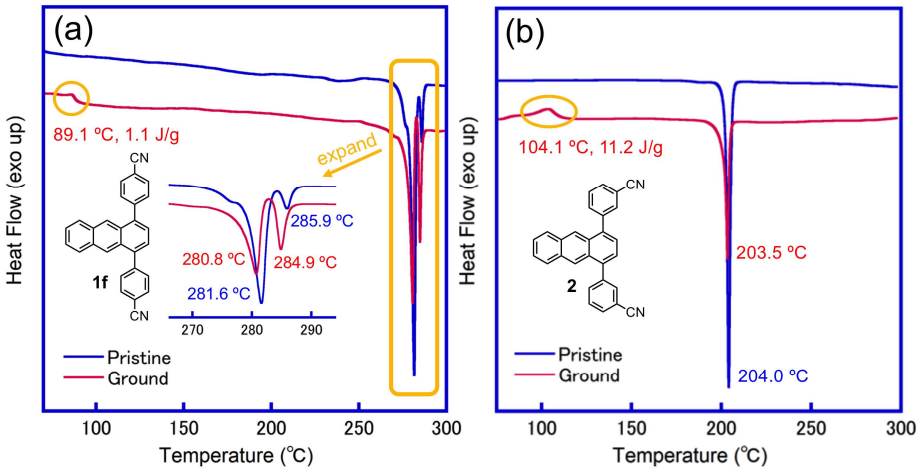


Figure 9. DSC profiles of 1,4-diphenylanthracene derivatives before grinding (pristine) and after grinding (ground): (**a**) **1f** (R = CN), (**b**) **2** (3-CN).

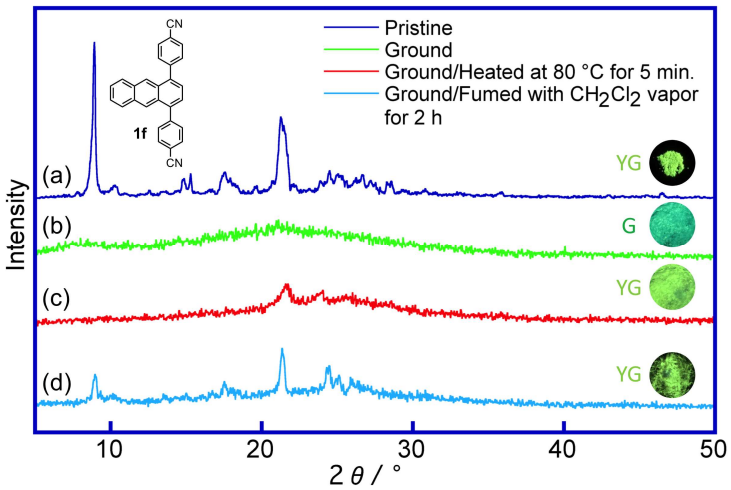
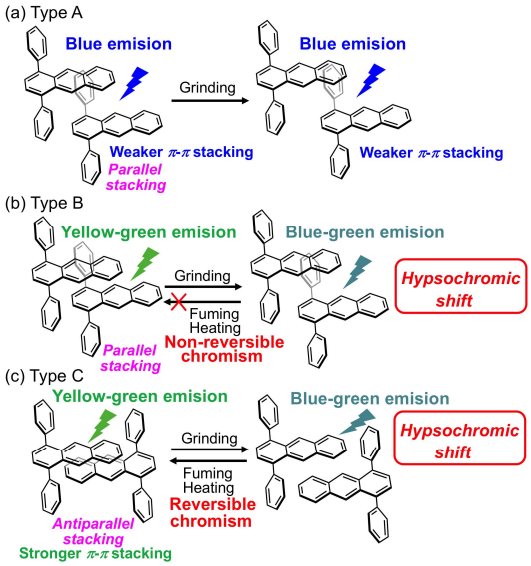


Figure 10. Powder X-ray diffraction (PXRD) patterns of 1,4-diphenylanthracene derivative **1f** (R = CN): (**a**) pristine, (**b**) ground, (**c**) ground-heated sample (80 °C, 5 min.), and (**d**) ground-fumed sample (with CH_2Cl_2 vapor, 2 h).

Furthermore, the IR spectra of the ground-heated and ground-fumed samples showed a recovery of the wavenumber of the CN stretching bands from the ground state in derivatives **1f** and **2** (a shorter wavenumber shift from the ground sample was observed; Figures 6, S10 and S11), and only the CN-substituted 1,4-diphenylanthracene derivatives showed a reversible emission color change, indicating that the hydrogen bond between the Ar–CN group and the Ar–H hydrogen atom (Ar–CN· · · H–Ar) is important for the controllable reversible mechanofluorochromism in the CN-substituted 1,4-diphenylanthracene derivatives.

Although it is difficult to further understand the critical mechanism of this mechanofluorochromism, it can be classified as follows: (Type-A) the 1,4-diphenylanthracene derivatives **1a**–**1c** show a blue luminous color in the pristine state, and the crystal packing showed a parallel-type orientation. Only a weaker π–π stacking was observed, and its blue luminous color probably comes from monomer emission. After grinding the pristine sample, it does not change the original luminous color (Scheme 2a); (Type-B) the derivatives **1d**, **1e,** and **4** show green and yellow-green luminous colors in the pristine state, and the crystal packing of **1d** showed a parallel-type orientation. Only weak π–π stacking was observed, and its green and yellow-green luminous color probably comes from the partial excimer emission or charge-transfer interactions. After grinding the pristine sample, it changes its original luminous color to a bluish color, but its original luminous color does not recover by heating and fuming of the ground samples (Scheme 2b); (Type-C) the derivatives **1f**, **2,** and **3**, which having CN-groups, show a yellow-green luminous color in the pristine state, and the crystal packing showed an antiparallel-type orientation. A stronger π–π stacking was observed, and its yellow-green luminous color probably comes from the excimer emission. After grinding the pristine sample, its original luminous color changes to the shorter wavelength side (yellow-green to green or yellow-green to blue-green), and its original luminous color was repeatedly recovered by heating and fuming of the ground samples. Thus, only some of the CN-substituted 1,4-diphenylanthracene derivatives exhibited a repetitive reversible mechanofluorochromism with a "*hypsochromic*" luminous color change upon grinding, heating, and fuming with solvent vapors, which may be due to the stronger π–π stacking attributed to the antiparallel crystal packing structure (Scheme 2c). The mechanofluorochromic properties of other phenylanthracence derivatives, such as 1,5-diphenylanthracence and fused phenylanthracene derivatives [111] are currently under investigation.



Scheme 2. Schematic diagram of different types of mechanofluorochromic properties of 1,4-diphenylanthracene derivatives: (**a**) Type-A, non-mechanofluorochromic phenomenon for derivatives **1a**–**1c**; (**b**) Type-B shows mechanofluorochromic phenomenon but non-reversible change by fuming and heating for derivatives **1d**, **1e,** and **4**; (**c**) Type-C shows mechanofluorochromic phenomenon repeatedly changing by fuming and heating for the CN-substituted derivatives **1f**, **2,** and **3**.

3. Materials, Equipment and Methods

3.1. General Methods

The ^{1}H and ^{13}C NMR spectra were recorded using Bruker (Billerica, MA, USA) Avance III (^{1}H: 500 and ^{13}C: 125 MHz) spectrometers. The FAB-mass spectra were recorded by a JEOL (Tokyo, Japan) JMS-700 mass spectrometer. The absorption spectra (solid and

solution samples) were recorded by a Jasco (Tokyo, Japan) V-750 UV-Visible spectrometer. The fluorescence spectra for the solution samples were recorded by a Jasco (Tokyo, Japan) FP-8300 spectrometer, and the fluorescence spectra were calibrated using rhodamine B as the reference. The fluorescence spectra for the solid samples were recorded by a Flame-S, Ocean Optics (Orlando, FL, USA) fiber-optic spectrometer (λ_{ex} = 365 nm). The absolute PL quantum yields (Φ) were determined by a Quantaurus-QY (Hamamatsu Photonics, Hamamatsu, Japan) instrument. The emission lifetimes were measured by a Quantaurus-Tau (Hamamatsu Photonics) instrument. The DSC thermograms of the solid samples were recorded by a TA Instruments (New Castle, Delaware, USA) DSC 2920 modulated DSC and were recorded at the constant heating rate of 10 °C/min. The infrared spectra were recorded using a Jasco (Tokyo, Japan) FTIR 4600 spectrometer equipped with an attenuated total reflection (ATR) unit. All the solvents and reagents were purified according to standard procedures. 3,5-dicyanophenylboronic acid [65] and 1,4-dibromoanthracene [112–114] were prepared according to published procedure.

3.2. Synthesis of 1,4-Diphenylanthracene Derivatives **1–4**

General Procedure: 1,4-dibromoanthracene (103 mg, 0.307 mmol), phenylboronic acid (90.6 mg, 0.743 mmol), $Pd(PPh_3)_4$ (35.6 mg, 30.8 μmol) were mixed in 20 mL of DME. Then a 1 M K_2CO_3 aqueous solution (3.0 mL, 3.00 mmol) was added. The obtained mixture was degassed 3 times by a freeze-pump-through method, and then the mixture was heated at 85 °C for 18 h under an Ar atmosphere. After removing the solvent in vacuo and adding water (80 mL), the mixture was extracted with CH_2Cl_2 (80 mL), dried over anhydrous Na_2SO_4, and the solvent evaporated. The 1,4-diphenylanthracene **1a** was isolated (98.2 mg, 97%) by column chromatography (SiO_2, CH_2Cl_2, or CH_2Cl_2/hexane) followed by recrystallization from MeOH or CH_2Cl_2/MeOH.

1a (R = H): yield 87%, pale-yellow needles, mp: 157.8–158.8 °C; ^{1}H NMR (500 MHz, $CDCl_3$): δ (ppm) = 8.52 (s, 2H), 7.87 (dd, J = 6.4, 3.3 Hz, 2H), 7.63 (d, J = 8.2 Hz, 4H), 7.56 (t, J = 7.5 Hz, 4H), 7.49 (t, J = 7.3 Hz, 2H), 7.44 (s, 2H), 7.40 (dd, J = 6.6, 3.2 Hz, 2H), ^{13}C NMR (125 MHz, $CDCl_3$): δ (ppm) = 141.2 (Cq), 140.0 (Cq), 131.5 (Cq), 130.8 (Cq), 130.4 (CH), 128.6 (CH), 128.5 (CH), 127.6 (CH), 125.9 (CH), 125.7 (CH), 125.5 (CH), HRMS (FAB, NBA) m/z = 330.1417 (calculated for $M^{+\cdot}$: 330.1409), Anal. Calcd. for $C_{26}H_{18}$: C: 94.51, H: 5.49, Found: C: 94.41, H: 5.58.

1b (R = Me): yield 76%, pale-yellow prisms, mp: 192.3–193.3 °C; ^{1}H NMR (500 MHz, $CDCl_3$): δ (ppm) = 8.54 (s, 2H), 7.87 (dd, J = 6.4, 3.3 Hz, 2H), 7.52 (d, J = 8.0 Hz, 4H), 7.42 (s, 2H), 7.39 (dd, J = 6.6, 3.2 Hz, 2H), 7.37 (d, J = 7.7 Hz, 4H), 2.50 (s, 6H), ^{13}C NMR (125 MHz, $CDCl_3$): δ (ppm) = 139.6 (C_q), 138.1 (C_q), 137.1 (C_q), 131.3 (C_q), 130.7 (C_q), 130.1 (CH), 129.1 (CH), 128.3 (CH), 125.8 (CH), 125.4 (CH), 125.3 (CH), 21.3 (CH_3), HRMS (FAB, NBA) m/z = 358.1723 (calculated for $M^{+\cdot}$: 358.1722), Anal. Calcd. for $C_{28}H_{22}\cdot 0.4H_2O$: C: 91.97, H: 6.28, Found: C: 92.02, H: 6.17.

1c (R = F): yield 94%, pale-yellow prisms, mp: 160.0–161.0 °C; ^{1}H NMR (500 MHz, $CDCl_3$): δ (ppm) = 8.43 (s, 2H), 7.87 (dd, J = 6.4, 3.3 Hz, 2H), 7.55 (m, 4H), 7.42 (dd, J = 6.6, 3.2 Hz, 2H), 7.38 (s, 2H), 7.24 (m, 4H), ^{13}C NMR (125 MHz, $CDCl_3$): δ (ppm) = 162.6 (C_q, d, $^1J_{C\text{-}F}$ = 246.7 Hz), 139.1 (C_q), 136.9 (C_q, d, $^4J_{C\text{-}F}$ = 3.0 Hz), 131.9 (CH), 131.8 (CH), 131.6 (C_q), 130.8 (C_q), 128.4 (CH), 126.0 (CH), 125.3 (CH), 115.6 (CH, d, $^2J_{C\text{-}F}$ = 21.4 Hz), ^{19}F NMR (470 MHz, $CDCl_3$): δ (ppm) = −116.1, HRMS (FAB, NBA) m/z = 366.1230 (calculated for $M^{+\cdot}$: 366.1220), Anal. Calcd. for $C_{26}H_{16}F_2$: C: 85.23, H: 4.40, Found: C: 85.15, H: 4.46.

1d (R = OMe): yield 80%, yellow solids, mp: 246.9–247.9 °C; ^{1}H NMR (500 MHz, $CDCl_3$): δ (ppm) = 8.53 (s, 2H), 7.88 (dd, J = 6.4, 3.3 Hz, 2H), 7.54 (d, J = 8.7 Hz, 4H), 7.404 (s, 2H), 7.401 (dd, J = 6.4, 3.3 Hz, 2H), 7.10 (d, J = 8.7 Hz, 4H), 3.93 (s, 6H), ^{13}C NMR (125 MHz, $CDCl_3$): δ (ppm) = 159.2 (C_q), 139.4 (C_q), 133.6 (C_q), 131.5 (C_q), 131.4 (CH), 131.1 (C_q), 128.5 (CH), 125.9 (CH), 125.6 (CH), 125.5 (CH), 114.0 (CH), 55.5 (CH_3), HRMS (FAB, NBA) m/z = 390.1619 (calculated for $M^{+\cdot}$: 390.1620), Anal. Calcd. for $C_{28}H_{24}O_3\cdot H_2O$: C: 82.33, H: 5.92, Found: C: 82.30, H: 5.57.

1e (R = CF_3): yield 88%, yellow solids, mp: 207.5–208.5 °C; ^{1}H NMR (500 MHz, $CDCl_3$): δ (ppm) = 8.42 (s, 2H), 7.89 (dd, J = 6.4, 3.2 Hz, 2H), 7.83 (d, J = 8.0 Hz, 4H), 7.73 (d, J = 8.0 Hz, 4H), 7.45 (dd, J = 6.6, 3.1 Hz, 2H), 7.43 (s, 2H), ^{13}C NMR (125 MHz, $CDCl_3$): δ (ppm) = 144.5 (C_q), 139.1 (C_q), 131.6 (C_q), 130.5 (CH), 130.1 (C_q), 129.83 (q, $^2J_{C\text{-}F}$ = 32.5 Hz), 128.3 (CH), 126.1 (CH), 125.8 (CH), 125.5 (CH, q, $^3J_{C\text{-}F}$ = 3.6 Hz), 125.1 (CH), 124.3 (CF_3, q, $^1J_{C\text{-}F}$ = 272.1 Hz), ^{19}F NMR (470 MHz, $CDCl_3$): δ (ppm) = −63.5, HRMS (FAB, NBA) m/z = 466.1154 (calculated for $M^{+\cdot}$: 466.1156), Anal. Calcd. for $C_{28}H_{16}F_6 \cdot 0.2H_2O$: C: 71.55, H: 3.52, Found: C: 71.41, H: 3.50.
1f (R = CN): yield 88%, yellow solids, mp: 278.5–279.5 °C; ^{1}H NMR (500 MHz, $CDCl_3$): δ (ppm) = 8.39 (s, 2H), 7.90 (dd, 2H), 7.89 (d, J = 8.2 Hz, 4H), 7.75 (d, J = 8.2 Hz, 4H), 7.49 (dd, J = 6.6, 3.2 Hz, 2H), 7.45 (s, 2H), ^{13}C NMR (125 MHz, $CDCl_3$): δ (ppm) = 145.5 (C_q), 139.0 (C_q), 132.4 (CH), 131.7 (C_q), 130.8 (CH), 129.7 (C_q), 128.2 (CH), 126.4 (CH), 125.8 (CH), 125.0 (CH), 118.8 (C_q), 111.6 (C_q), HRMS (FAB, NBA) m/z = 380.1324 (calculated for $M^{+\cdot}$: 380.1313), Anal. Calcd. for $C_{28}H_{16}N_2 \cdot 0.2H_2O$: C: 87.57, H: 4.30, N: 7.29, Found: C: 87.51, H: 4.37, N: 7.17.
2 (3-CN): yield 88%, yellow solids, mp: 208.1–209.1 °C; ^{1}H NMR (500 MHz, $CDCl_3$): δ (ppm) = 8.35 (s, 2H), 7.92 (t, J = 1.6 Hz, 2H), 7.92 (dd, 2H), 7.87 (dt, J = 7.7, 1.5 Hz, 2H), 7.83 (dt, J = 7.8, 1.4 Hz, 2H), 7.50 (dd, J = 6.6, 3.2 Hz, 2H), 7.43 (s, 2H), ^{13}C NMR (125 MHz, $CDCl_3$): δ (ppm) = 141.9 (C_q), 138.4 (C_q), 134.5 (CH), 133.5 (CH), 131.7 (C_q), 131.3 (CH), 129.9 (C_q), 129.4 (CH), 128.2 (CH), 126.4 (CH), 125.9 (CH), 124.9 (CH), 118.7 (C_q), 112.9 (C_q), HRMS (FAB, NBA) m/z = 380.1306 (calculated for $M^{+\cdot}$: 380.1313), Anal. Calcd. for $C_{28}H_{16}N_2 \cdot 0.4H_2O$: C: 86.75, H: 4.37, N: 7.23, Found: C: 86.65, H: 4.29, N: 7.12.
3 (3,5-CN_2, R′=CN): yield 45%, yellow solids, mp: >300 °C; ^{1}H NMR (500 MHz, $CDCl_3$): δ (ppm) = 8.24 (s, 2H), 8.13 (d, J = 1.5 Hz, 4H), 8.11 (t, J = 1.5 Hz, 2H), 7.95 (dd, J = 6.5, 3.3 Hz, 2H), 7.58 (dd, J = 6.6, 3.1 Hz, 2H), 7.44 (s, 2H), ^{13}C NMR (125 MHz, $CDCl_3$): δ (ppm) = 143.3 (C_q), 137.2 (CH), 137.0 (C_q), 134.5 (CH), 132.1 (C_q), 129.2 (C_q), 128.2 (CH), 127.2 (CH), 126.2 (CH), 124.6 (CH), 116.5 (C_q), 114.7 (C_q), HRMS (FAB, NBA) m/z = 430.1214 (calculated for $M^{+\cdot}$: 430.1218).
4 (3,5-F_2, R′ = F): yield 99%, yellow solids, mp: 196.8–197.8 °C; ^{1}H NMR (500 MHz, $CDCl_3$): δ (ppm) = 8.45 (s, 2H), 7.92 (dd, J = 6.4, 3.3 Hz, 2H), 7.47 (dd, J = 6.6, 3.1 Hz, 2H), 7.40 (s, 2H), 7.13 (dd, $^3J_{F\text{-}H}$ = 7.8 Hz, $^4J_{H\text{-}H}$ = 2.0 Hz, 4H), 6.96 (tt, $^3J_{F\text{-}H}$ = 9.0 Hz, $^4J_{H\text{-}H}$ = 2.3 Hz, 2H), ^{13}C NMR (125 MHz, $CDCl_3$): δ (ppm) = 163.2 (C_q, dd, $^1J_{C\text{-}F}$ = 249.1, $^3J_{C\text{-}F}$ = 12.9 Hz), 144.1 (C_q, t, $^3J_{C\text{-}F}$ = 9.5 Hz), 138.6 (C_q), 131.9 (C_q), 130.0 (C_q), 128.5 (CH), 126.4 (CH), 125.7 (CH), 125.1 (CH), 113.3 (CH, dd, $^2J_{C\text{-}F}$ = 19.3, $^4J_{C\text{-}F}$ = 6.1 Hz), 103.3 (CH, t, $^2J_{C\text{-}F}$ = 25.3 Hz), ^{19}F NMR (470 MHz, $CDCl_3$): δ (ppm) = −110.8, HRMS (FAB, NBA) m/z = 402.1045 (calculated for $M^{+\cdot}$: 402.1032), Anal. Calcd. for $C_{26}H_{14}F_4 \cdot 0.5H_2O$: C: 75.91, H: 3.68, Found: C:76.01, H: 3.75.

3.3. Computational Methods

Density functional theory (DFT) with the B3LYP functional at the 6–31G* basis set level was used to calculate the electro cloud distribution of the HOMO and LUMO in a vacuum. For the calculation from the obtained single crystal structures, two molecules, which were stacked on each other, were located, and the non-hydrogen atom coordinates were fixed. Only the hydrogen atoms were optimized to obtain the conformation for the DFT calculation. All of the calculations were performed using Gaussian 16W C.01 [115].

3.4. Crystallographic Analysis

Crystals suitable for X-ray crystallography were grown from the solutions of **1a** (R = H), **1c** (R = F) in hexane solution that were stored in a test tube and left to stand for several days. For compounds **1d** (R = OMe) and **1f** (R = CN), the crystals were obtained from DME solution. For compounds **1b** (R = Me) and **2** (3-CN), the crystals were obtained from CH_2Cl_2 and $CHCl_3$ solutions, respectively. For the crystallographic data collection of **1a** (R = H) and **2** (3-CN), Rigaku XtaLAB mini with graphite-monochromated Mo-Kα radiation was used. Calculations were performed using the Olex2, version 1.3.0 crystallographic

software packages [116]. The crystal structures were solved by a direct method using Shelxt Version 2014/2015 [117,118]. The structure refinements were performed by a full-matrix least squares method using Shelxl Version 2014/2015 [119,120]. For the crystallographic data collection of **1b** (R = Me), **1c** (R = F), **1d** (R = OMe), and **1f** (R = CN), a Bruker D8 VENTURE equipped with a rotating anode of Mo-Kα or Cu-Kα radiation and a PHOTON III detector was used. Calculations were performed using the Bruker APEX3, 2019 [121] software package. Details of the data are summarized in Tables S3 and S4. All non-hydrogen atoms were anisotropically refined. All the hydrogen atoms were placed in idealized positions and were included in the structure factor calculations but were not refined. CCDC-2314555-2314560 contains the supplementary crystallographic data for this paper. These data can be obtained free of charge from The Cambridge Crystallographic Data Centre.

3.5. PXRD Analysis

Powder X-ray diffraction (PXRD) patterns of the samples were recorded using a Rigaku Smartlab X-ray diffractometer with CuK_α radiation (1.5406 Å) at a voltage of 40 kV and a current of 30 mA, and the data were collected with a step size of 0.01° over a 2θ range of 5–50°.

4. Conclusions

In this study, several types of 1,4-diphenylanthracene derivatives **1**–**4** were prepared, and their photophysical properties were observed in the solid and solution states. The CN-group substituted 1,4-diphenylanthracene derivative **2** exhibited a relatively high fluorescence quantum yield (Φ = 0.71) in the solid state than that in the solution state. Interestingly, for some derivatives, an increase in the fluorescence quantum yield was observed in the PMMA film (1 wt%) over both the solid state and the solution state. More interestingly, some of the 1,4-diphenylanthracene derivatives exhibited mechanofluorochromic properties with "*hypsochromic shift*" of the luminous color depending on the substituents of the phenyl group. Especially for some CN-substituted derivatives, a reversible luminous color change with a "*hypsochromic shift*" was observed, probably due to the formation of the antiparallel-type packing structure. These "*hypsochromic*" anthracene derivatives could probably be applied as new mechanofluorochromic materials.

Supplementary Materials: The following supporting information can be downloaded at: https://www.mdpi.com/article/10.3390/molecules29020407/s1. Fluorescence spectra of the pristine, ground, and stored samples of 1,4-diphenylanthracene derivatives (Figure S1), fluorescence images of the pristine, ground, stored, heated and fumed sample of 1,4-diphenylanthracene derivatives (Figures S2 and S3), normalized fluorescence spectra of the pristine, ground, ground-fumed and ground-heated samples (Figure S4), vapochromic properties of 1,4-diphenylanthracene derivatives (Figures S5 and S6), thermochromic properties of 1,4-diphenylanthracene derivatives (Figures S7–S9), IR spectra of the CN-substituted 1,4-diphenylanthracene derivatives (Figures S10 and S11), DSC profiles of 1,4-diphenylanthracene derivatives (Figure S12), UV-vis absorption spectra of the pristine and ground samples (Figure S13), UV-vis absorption spectra of 1,4-diphenylanthracene derivatives in solution (Figure S14), fluorescence spectra of 1,4-diphenylanthracene derivatives in solution (Figures S15–S17), fluorescence spectra of 1,4-diphenylanthracene derivatives in PMMA film (Figures S18 and S19), fluorescence lifetime decay profiles of pristine, ground, ground-heated and ground-fumed samples (Figure S20), fluorescence lifetime decay profiles of 1,4-diphenylanthracene derivatives in solution (Figure S21), fluorescence lifetime decay profiles of 1,4-diphenylanthracene derivatives in PMMA film (Figure S22), photophysical properties of 1,4-diphenylanthracene derivatives (Tables S1 and S2), single crystal X-ray analysis of 1,4-diphenylanthracene derivatives (Tables S3 and S4, Figures S23–S37), Powder X-ray diffraction (PXRD) patterns (Figure S38), DFT calculation of the obtained crystal structures (Figures S39–S42), UV irradiation experiments for 1,4-diphenylanthracene derivatives (Figures S43 and S44), andNMR spectra of new compounds.

Author Contributions: F.K. experiment, formal analysis, data curating, computation, and writing. T.A. experiment, formal analysis, data curating, M.N. experiment, formal analysis, K.Y. crystallographic analysis, T.K. design, supervision, editing, project administration, and writing-review and editing. All authors have read and agreed to the published version of the manuscript.

Funding: This research received no external funding.

Institutional Review Board Statement: Not applicable.

Informed Consent Statement: Not applicable.

Data Availability Statement: Data are contained within the article and supplementary materials.

Acknowledgments: We thank K. Naka and H. Imoto (Kyoto Institute of Technology) for the single crystal X-ray analysis. This study was the result of using research equipment shared in the MEXT Project for promoting public utilization of advanced research infrastructure (program for supporting the introduction of the new sharing system) Grant Number JPMXS0421800120.

Conflicts of Interest: Author Kenji Yoza was employed by the company Bruker Japan K.K. The remaining authors declare that the research was conducted in the absence of any commercial or financial relationships that could be construed as a potential conflict of interest.

References

1. Aziz, H.; Popovic, Z.D.; Hu, N.-X.; Hor, A.-M.; Xu, G. Degradation Mechanism of Small Molecule–Based Organic Light-Emitting Devices. *Science* **1999**, *283*, 1900. [CrossRef] [PubMed]
2. Friend, R.H.; Gymer, R.W.; Holmes, A.B.; Burroughes, J.H.; Marks, R.N.; Taliani, C.; Bradley, D.D.C.; Santos, D.A.D.; Brédas, J.L.; Lögdlung, M.; et al. Electroluminescence in Conjugated Polymers. *Nature* **1999**, *397*, 121. [CrossRef]
3. Yanagi, H.; Morikawa, T.; Hotta, S. Electroluminescence from Low-Dimensionally Confined Crystals of Thiophene/*p*-Phenylene Co-Oligomers. *Appl. Phys. Lett.* **2002**, *81*, 1512. [CrossRef]
4. Lee, J.; Yuan, Y.-Y.; Kang, Y.; Jia, W.-L.; Lu, Z.-H.; Wang, S. 2,5-Functionalized Spiro-Bisiloles as Highly Efficient Yellow-Light Emitters in Electroluminescent Devices. *Adv. Funct. Mater.* **2006**, *16*, 681. [CrossRef]
5. Yuan, W.Z.; Lu, P.; Chen, S.; Lam, J.W.Y.; Wang, Z.; Liu, Y.; Kwok, H.S.; Ma, Y.; Tang, B.Z. Changing the Behavior of Chromophores from Aggregation-Caused Quenching to Aggregation-Induced Emission: Development of Highly Efficient Light Emitters in the Solid State. *Adv. Mater.* **2010**, *22*, 2159. [CrossRef] [PubMed]
6. Tang, M.L.; Bao, Z. Halogenated Materials as Organic Semiconductors. *Chem. Mater.* **2011**, *23*, 446. [CrossRef]
7. Yee, K.W.; Yokoyama, M.; Hiramoto, M. Very-Thin-Perylene-Crystal-Based Electroluminescent Devices. *Appl. Phys. Lett.* **2006**, *88*, 083511. [CrossRef]
8. Figueira-Duarte, T.M.; Müllen, K. Pyrene-Based Materials for Organic Electronics. *Chem. Rev.* **2011**, *111*, 7260. [CrossRef]
9. Gao, F.; Liano, Q.; Xu, Z.-Z.; Yue, Y.-H.; Wang, Q.; Zhang, H.-L.; Fu, H.-B. Strong Two-Photon Excited Fluorescence and Stimulated Emission from an Organic Single Crystal of an Oligo(Phenylene Vinylene). *Angew. Chem. Int. Ed.* **2010**, *49*, 732. [CrossRef]
10. Zhao, Y.S.; Peng, A.; Fu, H.; Ma, Y.; Yao, J. Nanowire Waveguides and Ultraviolet Lasers Based on Small Organic Molecules. *Adv. Mater.* **2008**, *20*, 1661. [CrossRef]
11. Bulovic, V.; Kozlov, V.G.; Khalfin, V.B.; Forrest, S.R. Transform-Limited, Narrow-Linewidth Lasing Action in Organic Semiconductor Microcavities. *Science* **1998**, *279*, 553. [CrossRef] [PubMed]
12. Duan, X.; Huang, Y.; Agarwal, R.; Lieber, C.M. Single-Nanowire Electrically Driven Lasers. *Nature* **2003**, *421*, 241. [CrossRef] [PubMed]
13. Schmidtke, J.; Stille, W.; Finkelmann, H.; Kim, S.T. Laser Emission in a Dye Doped Cholesteric Polymer Network. *Adv. Mater.* **2002**, *14*, 746–749. [CrossRef]
14. Samuel, I.D.W.; Turnbull, G.A. Organic Semiconductor Lasers. *Chem. Rev.* **2007**, *107*, 1272. [CrossRef] [PubMed]
15. Liao, Q.; Fu, H.; Yao, J. Waveguide Modulator by Energy Remote Relay from Binary Organic Crystalline Microtubes. *Adv. Mater.* **2009**, *21*, 4153. [CrossRef]
16. Tong, L.; Gattass, R.R.; Ashcom, J.B.; He, S.; Lou, J.; Shen, M.; Maxwell, I.; Mazur, E. Subwavelength-Diameter Silica Wires for Low-Loss Optical Wave Guiding. *Nature* **2003**, *426*, 816. [CrossRef]
17. Wang, X.; Zhou, Y.; Lei, T.; Hu, N.; Chen, E.-Q.; Pei, J. Structural-Property Relationship in Pyrazino[2,3-g]quinoxaline Derivatives: Morphology, Photophysical, and Waveguide Properties. *Chem. Mater.* **2010**, *22*, 3735. [CrossRef]
18. Takazawa, K.; Kitahama, Y.; Kimura, Y.; Kido, G. Optical Waveguide Self-Assembled from Organic Dye Molecules in Solution. *Nano. Lett.* **2005**, *5*, 1293. [CrossRef]
19. Zhang, C.; Zhao, Y.S.; Yao, J. Optical Waveguides at Micro/Nanoscale Based on Functional Small Organic Molecules. *Phys. Chem. Chem. Phys.* **2011**, *13*, 9060. [CrossRef]
20. Goyal, H.; Kumar, P.; Gupta, R. Polycyclic Aromatic Hydrocarbon-based Soft Materials: Applications in Fluorescent Detection, Gelation, AIEE and Mechanochromism. *Chem. Asian J.* **2023**, e202300355. [CrossRef]

21. Ito, S. Mechanochromic Luminescence of Soft Crystals: Recent Systematic Studies in Controlling the Molecular Packing and Mechanoresponsive Properties. *J. Photochem. Photobiol. C* **2022**, *51*, 100481. [CrossRef]
22. Sun, Y.; Lei, Z.; Ma, H. Twisted Aggregation-Induced Emission Luminogens (AIEgens) Contribute to Mechanochromism Materials: A Review. *J. Mater. Chem. C* **2022**, *10*, 14834. [CrossRef]
23. Mutai, T.; Takamizawa, S. Organic Soft Crystals Exhibiting Spontaneously Reversible Mechano-Responsive Luminescence. *J. Photochem. Photobiol. C* **2022**, *51*, 100479. [CrossRef]
24. Sagara, Y.; Kato, T. Mechanically Induced Luminescence Changes in Molecular Assemblies. *Nature Chem.* **2009**, *1*, 605. [CrossRef] [PubMed]
25. Yang, Z.; Chi, Z.; Mao, Z.; Zhang, Y.; Liu, S.; Zhao, J.; Aldred, M.P.; Chi, Z. Recent Advances in Mechano-Responsive Luminescence of Tetraphenylethylene Derivatives with Aggregation-Induced Emission Properties. *Mater. Chem. Front.* **2018**, *2*, 861. [CrossRef]
26. Luo, X.; Li, J.; Li, C.; Heng, L.; Dong, Y.Q.; Liu, Z.; Bo, Z.; Tang, B.Z. Reversible Switching of the Emission of Diphenyldibenzofulvenes by Thermal and Mechanical Stimuli. *Adv. Mater.* **2011**, *23*, 3261. [CrossRef] [PubMed]
27. Sagara, Y.; Yamane, S.; Mitani, M.; Weder, C.; Kato, T. Mechanoresponsive Luminescent Molecular Assemblies: An Emerging Class of Materials. *Adv. Mater.* **2016**, *28*, 1073. [CrossRef]
28. Huang, X.; Qian, L.; Zhou, Y.; Liu, M.; Cheng, Y.; Wu, H. Effective Structural Modification of Traditional Fluorophores to Obtain Organic Mechanofluorochromic Molecules. *J. Mater. Chem. C* **2018**, *6*, 5075. [CrossRef]
29. Xue, S.; Qiu, X.; Sun, Q.; Yang, W. Alkyl Length Effects on Solid-State Fluorescence and Mechanochromic Behavior of Small Organic Luminophores. *J. Mater. Chem. C* **2016**, *4*, 1568. [CrossRef]
30. Ito, H.; Saito, T.; Oshima, N.; Kitamura, N.; Ishizaka, S.; Hinatsu, Y.; Wakeshima, M.; Kato, M.; Tsuge, K.; Sawamura, M. Reversible Mechanochromic Luminescence of $[(C_6F_5Au)_2(\mu$-1,4-Diisocyanobenzene)]. *J. Am. Chem. Soc.* **2008**, *130*, 10044. [CrossRef]
31. Seki, T.; Kobayashi, K.; Ito, H. Low-Temperature-Selective Luminescent Mechanochromism of a Thienyl Gold Isocyanide Complex. *Chem. Commun.* **2017**, *53*, 6700. [CrossRef]
32. Li, H.; Wang, Y.; Xu, Z. Reversible Mechanochromic Studies on AIE-Inspired Smart Materials and Their Applications in HCHO Sensing. *Dalton Trans.* **2022**, *51*, 6332. [CrossRef] [PubMed]
33. Peng, D.; He, L.-H.; Ju, P.; Chen, J.-L.; Ye, H.-Y.; Wang, J.-Y.; Liu, S.-J.; Wen, H.-R. Reversible Mechanochromic Luminescence of Tetranuclear Cuprous Complexes. *Inorg. Chem.* **2020**, *59*, 17213. [CrossRef] [PubMed]
34. Liu, L.; Wen, T.; Fu, W.-Q.; Liu, M.; Chen, S.; Zhang, J. Structure-Dependent Mechanochromism of Two Ag(I) Imidazolate Chains. *CrystEngComm* **2016**, *18*, 218. [CrossRef]
35. Geng, H.; Luo, K.; Zou, G.; Wang, H.; Ni, H.; Yu, W.; Li, Q.; Wang, Y. New Phosphorescent Platinum(II) Complexes: Lamellar Mesophase and Mechanochromism. *New J. Chem.* **2016**, *40*, 10371. [CrossRef]
36. Seki, T.; Takamatsu, Y.; Ito, H. A Screening Approach for the Discovery of Mechanochromic Gold(I) Isocyanide Complexes with Crystal-To-Crystal Phase Transitions. *J. Am. Chem. Soc.* **2016**, *138*, 6252. [CrossRef]
37. Ai, Y.; Li, Y.; Chan, M.H.-Y.; Xiao, G.; Zou, B.; Yam, V.W.-W. Realization of Distinct Mechano- and Piezochromic Behaviors Via Alkoxy Chain Length-Modulated Phosphorescent Properties and Multidimensional Self-Assembly Structures of Dinuclear Platinum(II) Complexes. *J. Am. Chem. Soc.* **2021**, *143*, 10659. [CrossRef]
38. Seki, T.; Ida, K.; Ito, H. A Meta-Diisocyanide Benzene-Based Aryl Gold Isocyanide Complex Exhibiting Multiple Solid-State Molecular Arrangements and Luminescent Mechanochromism. *Mater. Chem. Front.* **2018**, *2*, 1195. [CrossRef]
39. Zhao, K.-Y.; Shan, G.-G.; Fu, Q.; Su, Z.-M. Tuning Emission of AIE-Active Organometallic Ir(III) Complexes by Simple Modulation of Strength of Donor/Acceptor on Ancillary Ligands. *Organometallics* **2016**, *35*, 3996. [CrossRef]
40. Yagai, S.; Seki, T.; Aonuma, H.; Kawaguchi, K.; Karatsu, T.; Okura, T.; Sakon, A.; Uekusa, H.; Ito, H. Mechanochromic Luminescence Based on Crystal-To-Crystal Transformation Mediated by a Transient Amorphous State. *Chem. Mater.* **2016**, *28*, 234. [CrossRef]
41. Chen, Z.; Liu, G.; Wang, R.; Pu, S. Highly Emissive Carbazole-Based Gold(I) Complex with a Long Room-Temperature Phosphorescence Lifetime and Self-Reversible Mechanochromism Characteristics. *RSC Adv.* **2017**, *7*, 15112. [CrossRef]
42. Huitorel, B.; Benito, Q.; Fargues, A.; Garcia, A.; Gacoin, T.; Boilot, J.-P.; Perruchas, S.; Camerel, F. Mechanochromic Luminescence and Liquid Crystallinity of Molecular Copper Clusters. *Chem. Mater.* **2016**, *28*, 8190. [CrossRef]
43. Jin, M.; Seki, T.; Ito, H. Luminescent Mechanochromism of a Chiral Complex: Distinct Crystal Structures and Color Changes of Racemic and Homochiral Gold(I) Isocyanide Complexes with a Binaphthyl Moiety. *Chem. Commun.* **2016**, *52*, 8083. [CrossRef] [PubMed]
44. Seki, T.; Tokodai, N.; Omagari, S.; Nakanishi, T.; Hasegawa, Y.; Iwasa, T.; Taketsugu, T.; Ito, H. Luminescent Mechanochromic 9-Anthryl Gold(I) Isocyanide Complex with an Emission Maximum at 900 nm After Mechanical Stimulation. *J. Am. Chem. Soc.* **2017**, *139*, 6514. [CrossRef] [PubMed]
45. Dong, Y.; Xu, B.; Zhang, J.; Tan, X.; Wang, L.; Chen, J.; Lv, H.; Wen, S.; Li, B.; Ye, L.; et al. Piezochromic Luminescence Based on the Molecular Aggregation of 9,10-Bis((*E*)-2-(pyrid-2-yl)vinyl)anthracene. *Angew. Chem. Int. Ed.* **2012**, *51*, 10782. [CrossRef] [PubMed]
46. Tu, D.; Leong, P.; Li, Z.; Hu, R.; Shi, C.; Zhang, K.Y.; Yan, H.; Zhao, Q. A Carborane-Triggered Metastable Charge Transfer State Leading to Spontaneous Recovery of Mechanochromic Luminescence. *Chem. Commun.* **2016**, *52*, 12494. [CrossRef]
47. Li, H.; Zhang, X.; Chi, Z.; Xu, B.; Zhou, W.; Liu, S.; Zhang, Y.; Xu, J. New Thermally Stable Piezofluorochromic Aggregation-Induced Emission Compounds. *Org. Lett.* **2011**, *13*, 556. [CrossRef]

48. Wu, X.; Guo, J.; Cao, Y.; Zhao, J.; Jia, W.; Chen, Y.; Jia, D. Mechanically Triggered Reversible Stepwise Tricolor Switching and Thermochromism of Anthracene-*o*-Carborane Dyad. *Chem. Sci.* **2018**, *9*, 5270. [CrossRef]
49. Li, R.; Xiao, S.; Li, Y.; Lin, Q.; Zhang, R.; Zhao, J.; Yang, C.; Zou, K.; Li, D.; Yi, T. Polymorphism-Dependent and Piezochromic Luminescence Based on Molecular Packing of a Conjugated Molecule. *Chem. Sci.* **2014**, *5*, 3922. [CrossRef]
50. Fedorenko, E.; Tretyakova, G.; Mirochnik, A.; Gerasimenko, A.; Beloliptsev, A. Anthracene-Containing Complexes of Boron Difluoride. Dual Luminescence, Formation of Excimers, and Mechanochromism. *Spectrochim. Acta A* **2021**, *262*, 120114. [CrossRef]
51. Suresh, S.K.; Raju, P.D.; Krishnan, A.; Ramachandran, L.M.; Suneesh, C.V. Supramolecular Interactions-Assisted Polymorphism and Unique Mechanofluorochromism in 9,10-Bis((*E*)-4-(trifluoromethyl)styryl)anthracene. *Chem. Eur. J.* **2023**, *29*, e202204030. [CrossRef] [PubMed]
52. Dai, Q.; Zhang, J.; Tan, R.; Wang, S.; Li, Y.; Li, Q.; Xiao, S. High-Contrast Reversible Mechanochromic Luminescence of a Conjugated Anthracene-Based Molecule. *Mater. Lett.* **2016**, *164*, 239. [CrossRef]
53. Xiong, Y.; Yan, X.; Ma, Y.; Li, Y.; Yin, G.; Chen, L. Regulating the Piezofluorochromism of 9,10-Bis(butoxystyryl)anthracenes by Isomerization of Butyl Groups. *Chem. Commun.* **2015**, *51*, 3403. [CrossRef]
54. Tanikubo, H.; Matsuo, T.; Hayashi, S. Alkyl-Chain Bridged Acrylonitrile-Appended Anthracene Chromophore Toward Mechanically-Induced Bathochromic Shift. *Bull. Chem. Soc. Jpn.* **2023**, *96*, 178. [CrossRef]
55. Naeem, K.C.; Subhakumari, A.; Varughese, S.; Nair, V.C. Heteroatom Induced Contrasting Effects on the Stimuli Responsive Properties of Anthracene Based Donor–π–Acceptor Fluorophores. *J. Mater. Chem. C* **2015**, *3*, 10225. [CrossRef]
56. Naito, H.; Morisaki, Y.; Chujo, Y. *o*-Carborane-Based Anthracene: A Variety of Emission Behaviors. *Angew. Chem. Int. Ed.* **2015**, *54*, 5084. [CrossRef]
57. Zhang, Z.; Yao, D.; Zhou, T.; Zhang, H.; Wang, Y. Reversible Piezo- and Photochromic Behaviors Accompanied by Emission Color Switching of Two Anthracene-Containing Organic Molecules. *Chem. Commun.* **2011**, *47*, 7782. [CrossRef] [PubMed]
58. Zheng, M.; Zhang, D.T.; Sun, M.X.; Li, Y.P.; Liu, T.L.; Xue, S.F.; Yang, W.J. Cruciform 9,10-Distyryl-2,6-Bis(*p*-dialkylamino-styryl)anthracene Homologues Exhibiting Alkyl Length-Tunable Piezochromic Luminescence and Heat-Recovery Temperature of Ground States. *J. Mater. Chem. C* **2014**, *2*, 1913. [CrossRef]
59. Bu, L.; Sun, M.; Zhang, D.; Liu, W.; Wang, Y.; Zheng, M.; Xue, S.; Yang, W. Solid-State Fluorescence Properties and Reversible Piezochromic Luminescence of Aggregation-Induced Emission-Active 9,10-Bis[(9,9-dialkylfluorene-2-yl)vinyl]anthracenes. *J. Mater. Chem. C* **2013**, *1*, 2028. [CrossRef]
60. Kohmoto, S.; Chuko, T.; Hisamatsu, S.; Okuda, Y.; Masu, H.; Takahashi, M.; Kishikawa, K. Piezoluminescence and Liquid Crystallinity of 4,4′-(9,10-Anthracenediyl)bispyridinium Salts. *Cryst. Growth Des.* **2015**, *15*, 2723. [CrossRef]
61. Gogoi, G.; Kashyap, D.; Sarma, R.J. Mechano-Luminescent Behavior of a Pyridine-Containing Anthracene Derivative: Role of Aromatic Stacking Interactions. *Cryst. Growth Des.* **2018**, *18*, 4963. [CrossRef]
62. Kusukawa, T.; Kojima, Y.; Kannen, F. Mechanofluorochromic Properties of 1,8-Diphenylanthracene Derivatives. *Chem. Lett.* **2019**, *48*, 1213. [CrossRef]
63. Kusukawa, T.; Kannen, F.; Kojima, Y.; Yoza, K. Crystal Polymorphism-Dependent Fluorescence of Fluoroarene-Substituted Anthracene Derivatives. *Chem. Lett.* **2021**, *50*, 31. [CrossRef]
64. Kusukawa, T.; Shibata, S.; Kannen, F.; Yoza, K. Mechnofluorochromic Properties of *N*-Alkyl Amide Anthracene Derivatives. *Tetrahedron* **2022**, *111*, 132735. [CrossRef]
65. Kannen, F.; Nishimura, M.; Yoza, K.; Kusukawa, T. Mechanofluorochromic Properties of 1-Phenylanthracene Derivatives with Extremely Simple Structures. *Tetrahedron* **2023**, *149*, 133710. [CrossRef]
66. Zhu, G.; Yu, T.; Chen, J.; Hu, R.; Yang, G.; Zeng, Y.; Li, Y. Dipyrene-Terminated Oligosilanes Enable Ratiometric Fluorescence Response in Polymers Toward Mechano- and Thermo-Stimuli. *ACS Appl. Mater. Interfaces.* **2023**, *15*, 11033. [CrossRef]
67. Sagara, Y.; Kato, T. Stimuli-Responsive Luminescent Liquid Crystals: Change of Photoluminescent Colors Triggered by a Shear-Induced Phase Transition. *Angew. Chem. Int. Ed.* **2008**, *47*, 5175. [CrossRef]
68. Ma, Z.; Teng, M.; Wang, Z.; Yang, S.; Jia, X. Mechanically Induced Multicolor Switching Based on a Single Organic Molecule. *Angew. Chem. Int. Ed.* **2013**, *52*, 12268. [CrossRef]
69. Zhang, H.; Chang, X.; Ma, C.; Huang, G.; Li, B.S.; Tang, B.Z. Two Cholesterol-Containing Pyrene Derivatives: Subtle Spacer Difference, Diverse Stimuli-Responsive Luminescence, Chirality, and Self-Assembly Behaviors. *ACS Appl. Mater. Interfaces* **2022**, *14*, 43926. [CrossRef]
70. Hirai, Y.; Laize-Générat, L.; Wrona-Piotrowicz, A.; Zakrzewski, J.; Makal, A.; Brosseau, A.; Michely, L.; Versace, D.-L.; Allain, C.; Métivier, R. Multi-Directional Mechanofluorochromism of Acetyl Pyrenes and Pyrenyl Ynones. *ChemPhysChem* **2021**, *22*, 1638. [CrossRef]
71. Li, W.; Wang, L.; Zhang, J.-P.; Wang, H. Bis-Pyrene-Based Supramolecular Aggregates with Reversibly Mechanochromic and Vapochromic Responsiveness. *J. Mater. Chem. C* **2014**, *2*, 1887. [CrossRef]
72. Teng, M.-J.; Jia, X.-R.; Yang, S.; Chen, X.-F.; Wei, Y. Reversible Tuning Luminescent Color and Emission Intensity: A Dipeptide-Based Light-Emitting Material. *Adv. Mater.* **2012**, *24*, 1255. [CrossRef] [PubMed]
73. Li, G.; Xu, Y.; Zhuang, W.; Wang, Y. Preparation of Organic Mechanochromic Fluorophores with Simple Structures and Promising Mechanochromic Luminescence Properties. *RSC Adv.* **2016**, *6*, 84787. [CrossRef]
74. Sagara, Y.; Mutai, T.; Yoshikawa, I.; Araki, K. Material Design for Piezochromic Luminescence: Hydrogen-Bond-Directed Assemblies of a Pyrene Derivative. *J. Am. Chem. Soc.* **2007**, *129*, 1520. [CrossRef]

75. Sagara, Y.; Komatsu, T.; Ueno, T.; Hanaoka, K.; Kato, T.; Nagano, T. Covalent Attachment of Mechanoresponsive Luminescent Micelles to Glasses and Polymers in Aqueous Conditions. *J. Am. Chem. Soc.* **2014**, *136*, 4273. [CrossRef] [PubMed]
76. Yu, Z.-D.; Dong, X.-X.; Cao, J.-Y.; Zhao, W.-X.; Bi, G.-H.; Wang, C.-Z.; Zhang, T.; Rahman, S.; Georghiou, P.E.; Lin, J.-B.; et al. Substituent Effects on the Intermolecular Interactions and Emission Behaviors in Pyrene-Based Mechanochromic Luminogens. *J. Mater. Chem. C* **2022**, *10*, 9310. [CrossRef]
77. Tong, J.; Wang, Y.; Mei, J.; Wang, J.; Qin, A.; Sun, J.Z.; Tang, B.Z. A 1,3-Indandione-Functionalized Tetraphenylethene: Aggregation-Induced Emission, Solvatochromism, Mechanochromism, and Potential Application as a Multiresponsive Fluorescent Probe. *Chem. Eur. J.* **2014**, *20*, 4661. [CrossRef]
78. Khan, F.; Ekbote, A.; Misra, R. Reversible Mechanochromism and Aggregation Induced Enhanced Emission in Phenothiazine Substituted Tetraphenylethylene. *New J. Chem.* **2019**, *43*, 16156. [CrossRef]
79. Zhang, G.-F.; Wang, H.; Aldred, M.P.; Chen, T.; Chen, Z.-Q.; Meng, X.; Zhu, M.-Q. General Synthetic Approach Toward Geminal-Substituted Tetraarylethene Fluorophores with Tunable Emission Properties: X-Ray Crystallography, Aggregation-Induced Emission and Piezofluorochromism. *Chem. Mater.* **2014**, *26*, 4433. [CrossRef]
80. Jia, J.; Zhao, H. Remarkable Isomeric Effects on the Mechanofluorochromism of Tetraphenylethylene-Based D–π–A Derivatives. *New J. Chem.* **2019**, *43*, 2231. [CrossRef]
81. Wang, X.; Qian, M.; Jiang, J.; Gao, Q.; Zhang, C.; Qi, H. Mechano-Chromic and Mechano-Enhanced Electrogenerated Chemiluminescence of Tetra[4-(4-cyanophenyl)phenyl]ethene. *Chem. Commun.* **2022**, *58*, 12847. [CrossRef] [PubMed]
82. Miao, X.; Cai, Z.; Zou, H.; Li, J.; Zhang, S.; Ying, L.; Deng, W. Achieving Halogen Bonding Enhanced Ultra-Highly Efficient AIE and Reversible Mechanochromism Properties of TPE-Based Luminogens: Position of Bromine Substituents. *J. Mater. Chem. C* **2022**, *10*, 8390. [CrossRef]
83. Wang, J.; Mei, J.; Hu, R.; Sun, J.Z.; Qin, A.; Tang, B.Z. Click Synthesis, Aggregation-Induced Emission, E/Z Isomerization, Self-Organization, and Multiple Chromisms of Pure Stereoisomers of a Tetraphenylethene-Cored Luminogen. *J. Am. Chem. Soc.* **2012**, *134*, 9956. [CrossRef] [PubMed]
84. Suenaga, K.; Tanaka, K.; Chujo, Y. Design and Luminescence Chromism of Fused Boron Complexes Having Constant Emission Efficiencies in Solution and in the Amorphous and Crystalline States. *Eur. J. Org. Chem.* **2017**, 5191. [CrossRef]
85. Taguchi, J.; Matsuura, S.; Seki, T.; Ito, H. Synthesis and Tunable Optical Properties of C,N-Chelated Borate Luminophores Derived from Potassium Acyltrifluoroborates. *Chem. Eur. J.* **2020**, *26*, 2450. [CrossRef] [PubMed]
86. Butler, T.; Morris, W.A.; Samonina-Kosicka, J.; Fraser, C.L. Mechanochromic Luminescence and Aggregation Induced Emission of Dinaphthoylmethane β-Diketones and Their Boronated Counterparts. *ACS Appl. Mater. Interfaces* **2016**, *8*, 1242. [CrossRef]
87. Qi, Y.; Wang, Y.; Ge, G.; Liu, Z.; Yu, Y.; Xue, M. Multi-State Emission Properties and the Inherent Mechanism of D–A–D Type Asymmetric Organic Boron Complexes. *J. Mater. Chem. C* **2017**, *5*, 11030. [CrossRef]
88. Potopnyk, M.A.; Kravets, M.; Luboradzki, R.; Volyniuk, D.; Sashuk, V.; Grazulevicius, J.V. Carbazole-Modified Thiazolo[3,2-c][1,3,5,2]oxadiazaborinines Exhibiting Aggregation-Induced Emission and Mechanofluorochromism. *Org. Biomol. Chem.* **2021**, *19*, 406. [CrossRef]
89. Morris, W.A.; Liu, T.; Fraser, C.L. Mechanochromic Luminescence of Halide-Substituted Difluoroboron β-Diketonate Dyes. *J. Mater. Chem. C* **2015**, *3*, 352. [CrossRef]
90. Liao, C.-W.; Rao, M.R.; Sun, S.-S. Structural Diversity of New Solid-State Luminophores Based on Quinoxaline-β-Ketoiminate Boron Difluoride Complexes with Remarkable Fluorescence Switching Properties. *Chem. Commun.* **2015**, *51*, 2656. [CrossRef]
91. Guo, C.; Li, M.; Yuan, W.; Wang, K.; Zou, B.; Chen, Y. Tuning the Mechanochromic Luminescence of BOPIM Complexes by Rational Introduction of Aromatic Substituents. *J. Phys. Chem. C* **2017**, *121*, 27009. [CrossRef]
92. Zhang, G.; Lu, J.; Sabat, M.; Fraser, C.L. Polymorphism and Reversible Mechanochromic Luminescence for Solid-State Difluoroboron Avobenzone. *J. Am. Chem. Soc.* **2010**, *132*, 2160. [CrossRef] [PubMed]
93. Qi, Y.; Liu, W.; Wang, Y.; Ma, L.; Yu, Y.; Zhang, Y.; Ren, L. The Inherent Mechanism of Mechanochromism Under Different Stress: Electron Cloud Density Distribution, J-Type Stacking, Pore Structure and Collapse of J-Type Stacking. *New J. Chem.* **2018**, *42*, 11373. [CrossRef]
94. Nguyen, N.D.; Zhang, G.; Lu, J.; Sherman, A.E.; Fraser, C.L. Alkyl Chain Length Effects on Solid-State Difluoroboron β-Diketonate Mechanochromic Luminescence. *J. Mater. Chem.* **2011**, *21*, 8409. [CrossRef]
95. Yoshii, R.; Suenaga, K.; Tanaka, K.; Chujo, Y. Mechanofluorochromic Materials Based on Aggregation-Induced Emission-Active Boron Ketoiminates: Regulation of the Direction of the Emission Color Changes. *Chem. Eur. J.* **2015**, *21*, 7231. [CrossRef] [PubMed]
96. Wu, J.; Cheng, Y.; Lan, J.; Wu, D.; Qian, S.; Yan, L.; He, Z.; Li, X.; Wang, K.; Zou, B.; et al. Molecular Engineering of Mechanochromic Materials by Programmed C−H Arylation: Making a Counterpoint in the Chromism Trend. *J. Am. Chem. Soc.* **2016**, *138*, 12803. [CrossRef]
97. Adak, A.; Panda, T.; Raveendran, A.; Bejoymohandas, K.S.; Asha, K.S.; Prakasham, A.P.; Mukhopadhyay, B.; Panda, M.K. Distinct Mechanoresponsive Luminescence, Thermochromism, Vapochromism, and Chlorine Gas Sensing by a Solid-State Organic Emitter. *ACS Omega* **2018**, *3*, 5291. [CrossRef]
98. Li, B.; Seth, K.; Niu, B.; Pan, L.; Yang, H.; Ge, H. Transient-Ligand-Enabled *ortho*-Arylation of Five-Membered Heterocycles: Facile Access to Mechanochromic Materials. *Angew. Chem. Int. Ed.* **2018**, *57*, 3401. [CrossRef]
99. Sagara, Y.; Kubo, K.; Nakamura, T.; Tamaoki, N.; Weder, C. Temperature-Dependent Mechanochromic Behavior of Mechanoresponsive Luminescent Compounds. *Chem. Mater.* **2017**, *29*, 1273. [CrossRef]

100. Panda, M.K.; Ravi, N.; Asha, P.; Prakasham, A.P. High Contrast Mechanochromic and Thermochromic Luminescence Switching by a Deep Red Emitting Organic Crystal. *CrystEngComm* **2018**, *20*, 6046. [CrossRef]
101. Yoshida, R.; Tachikawa, T.; Ito, S. Mechano- and Thermo-Responsive Luminescence of Crystalline Thienylbenzothiadiazole Derivatives: Stepwise Hypsochromic Switching of Near-Infrared Emission. *Cryst. Growth Des.* **2022**, *22*, 547. [CrossRef]
102. Chen, S.; Liu, W.; Zhang, W.; Ge, Z.; Wang, K.-P.; Gan, L.-H.; Hu, Z.-Q. Dimethylamine Substituted Bisbenzocoumarin Amides with Solvatochromic and Mechanochromic Properties. *Tetrahedron* **2019**, *75*, 3504. [CrossRef]
103. Nagura, K.; Saito, S.; Yusa, H.; Yamawaki, H.; Fujihisa, H.; Sato, H.; Shimoikeda, Y.; Yamaguchi, S. Distinct Responses to Mechanical Grinding and Hydrostatic Pressure in Luminescent Chromism of Tetrathiazolylthiophene. *J. Am. Chem. Soc.* **2013**, *135*, 10322. [CrossRef] [PubMed]
104. Seki, T.; Kobayashi, K.; Mashimo, T.; Ito, H. A Gold Isocyanide Complex with a Pendant Carboxy Group: Orthogonal Molecular Arrangements and Hypsochromically Shifted Luminescent Mechanochromism. *Chem. Commun.* **2018**, *54*, 11136. [CrossRef] [PubMed]
105. Chen, P.-Z.; Wang, J.-X.; Niu, L.-Y.; Chen, Y.-Z.; Yang, Q.-Z. Carbazole-Containing Difluoroboron β-Diketonate Dyes: Two-Photon Excited Fluorescence in Solution and Grinding-Induced Blue-Shifted Emission in the Solid State. *J. Mater. Chem. C* **2017**, *5*, 12538. [CrossRef]
106. Ying, S.; Chen, M.; Liu, Z.; Zheng, M.; Zhang, H.; Xue, S.; Yang, W. Unusual Mechanohypsochromic Luminescence and Unique Bidirectional Thermofluorochromism of Long-Alkylated Simple DPP Dyes. *J. Mater. Chem. C* **2017**, *5*, 5994. [CrossRef]
107. Khan, F.; Ekbote, A.; Singh, G.; Misra, R. Mechanochromic Luminogens with Hypsochromically Shifted Emission Switching Property: Recent Advances and Perspectives. *J. Mater. Chem. C* **2022**, *10*, 5024. [CrossRef]
108. Khan, F.; Urbonas, E.; Volyniuk, D.; Grazulevicius, J.V.; Mobin, S.M.; Misra, R. White Hyperelectrofluorescence from Solution-Processable OLEDs Based on Phenothiazine Substituted Tetraphenylethylene Derivatives. *J. Mater. Chem. C* **2020**, *8*, 13375. [CrossRef]
109. Nagai, S.; Yamashita, M.; Tachikawa, T.; Ubukata, T.; Asami, M.; Ito, S. Efficient and Versatile Mechanochromic Luminescence of Phenanthroimidazolylbenzothiadiazoles: Tricolor Switching and Directional Control over the Chromism. *J. Mater. Chem. C* **2019**, *7*, 4988. [CrossRef]
110. Wang, B.; Wu, Z.; Fang, B.; Yin, M. Blue-Shifted Mechanochromism of a Dimethoxynaphthalene-Based Crystal with Aggregation-Induced Emission. *Dyes Pigm.* **2020**, *182*, 108618. [CrossRef]
111. Kumar, G.J.; Bogoslavsky, B.; Debnath, S.; Bedi, A. Effect of Chalcogenophenes on Chiroptical Activity of Twisted Tetracenes: Computational Analysis, Synthesis and Crystal Structure Thereof. *Molecules* **2023**, *28*, 5074. [CrossRef]
112. Feofanov, M.; Akhmetov, V.; Sharapa, D.I.; Amsharov, K. Modular Approach to the Synthesis of Two-Dimensional Angular Fused Acenes. *Org. Lett.* **2020**, *22*, 1698. [CrossRef] [PubMed]
113. Wheeler, S.E.; McNeil, A.J.; Müller, P.; Swager, T.M.; Houk, K.N. Probing Substituent Effects in Aryl-Aryl Interactions Using Stereoselective Diels-Alder Cycloadditions. *J. Am. Chem. Soc.* **2010**, *132*, 3304. [CrossRef] [PubMed]
114. Tsvetkov, N.P.; Gonzalez-Rodriguez, E.; Hughes, A.; Gomes, G.D.P.; White, F.D.; Kuriakose, F.; Alabugin, I.V. Radical Alkyne Peri-Annulation Reactions for the Synthesis of Functionalized Phenalenes, Benzanthrenes, and Olympicene. *Angew. Chem. Int. Ed.* **2018**, *57*, 3651. [CrossRef] [PubMed]
115. Frisch, M.J.; Trucks, G.W.; Schlegel, H.B.; Scuseria, G.E.; Robb, M.A.; Cheeseman, J.R.; Scalmani, G.; Barone, V.; Petersson, G.A.; Nakatsuji, H.; et al. *Gaussian 16, Revision C.01*; Gaussian, Inc.: Wallingford, CT, USA, 2019.
116. *Olex2, Crystallographic Software Package*, version 1.3.0; OlexSys Ltd.: Durham, UK, 2024.
117. Sheldrick, G.M. SHELXT: Integrating Space Group Determination and Structure Solution. *Acta Crystallogr. Sect. A* **2014**, *70*, C1437. [CrossRef]
118. Sheldrick, G.M. Crystal Structure Refinement with SHELXL. *Acta Crystallogr. Sect. A* **2015**, *71*, 3–8. [CrossRef]
119. Sheldrick, G.M. A Short History of SHELX. *Acta Crystallogr. Sect. A* **2008**, *64*, 112. [CrossRef]
120. Sheldrick, G.M. SHELXT - Integrated Space-Group and Crystal-Structure Determination. *Acta Crystallogr. Sect. C* **2015**, *71*, 3–8. [CrossRef]
121. *APEX3*, Bruker AXS Inc.: Madison, WI, USA, 2019.

Disclaimer/Publisher's Note: The statements, opinions and data contained in all publications are solely those of the individual author(s) and contributor(s) and not of MDPI and/or the editor(s). MDPI and/or the editor(s) disclaim responsibility for any injury to people or property resulting from any ideas, methods, instructions or products referred to in the content.